Reviewer comments

Thomas Duc, Arthur Finez

June 25, 2026

1 Response to anonymous referee 1

This manuscript investigates the effect of yaw misalignment on wind turbine noise emissions through a full-scale acoustic measurement campaign. The experimental design addresses a relevant knowledge gap: quantifying acoustic implications of wake steering strategies increasingly deployed for power optimization. The study reports statistically significant directivity asymmetries that challenge omnidirectional noise source assumptions in current acoustic models, and observes a modest but consistent increase of approximately 0.6 dB(A) in overall sound power level under yaw misalignment. While the experimental approach is innovative and the dataset appears comprehensive, the manuscript suffers from insufficient justification of key methodological choices, inadequate discussion of contradictions with prior literature, and presentation issues that limit accessibility of the results.

The work represents a valuable contribution to the WFFC literature and provides high-quality data for model validation. The experimental design and dataset quality are strong, but methodological transparency, contradiction with prior literature, and presentation quality should be improved before publication. The authors should provide justification for processing parameter choices and discussion reconciling the current results in the context of past work in wind turbine aeroacoustics and directivity.

First, thank you very much for your positive feedback and the comprehensive review of the paper. We tried to account as much as possible to your suggestions in the revised version of the paper, as you can read in our comments below. We hope that these additions contribute to strengthen the scientific content of the paper.

1.1 Major Concerns

1. The observed increase in sound power under yaw misalignment appears to contradict past literature cited by the authors, which reported noise reductions or no significant effect from yaw misalignment. The authors cite these studies but offer no substantive discussion of why the current results diverge. Are the differences from turbine model, blade aerodynamics, study or measurement methodology?
A section has been added at the end of the paper to discuss results reported in the literature and propose some interpretation for the discrepancies. In addition to this section, rotor speed curves in Figure1 show that the curve with non-zero yaw are not generally below the $\beta = 0°$ case (except Yaw $+20°$ at 8 and 9 m/s). This is a possible reason for discrepancies with the main reference of NREL.

2. Time shifts of up to ±15 seconds are substantial relative to atmospheric turbulence timescales and microphone sampling frequency. The manuscript does not explain the root cause of such large clock drift over a four-day campaign. The cross-correlation procedure reduces uncertainty to approximately 1 second, but consequences for 10-second aggregated acoustic measurements remain unquantified. Given that acoustic propagation times span 1 second across the measurement domain, this uncertainty may not be negligible for directivity pattern analysis. Can the authors speculate on the impacts of the time delays as a source of measurement uncertainty? How does this influence the final results?
We run a sensitivity analysis on this effect by recalculating all results with an ±1 second offset on the acoustic data. As can be seen on Figure 2 below, the impact of this shift is negligible on the calculation of the directivity patterns and does not change the main conclusion of the paper. A

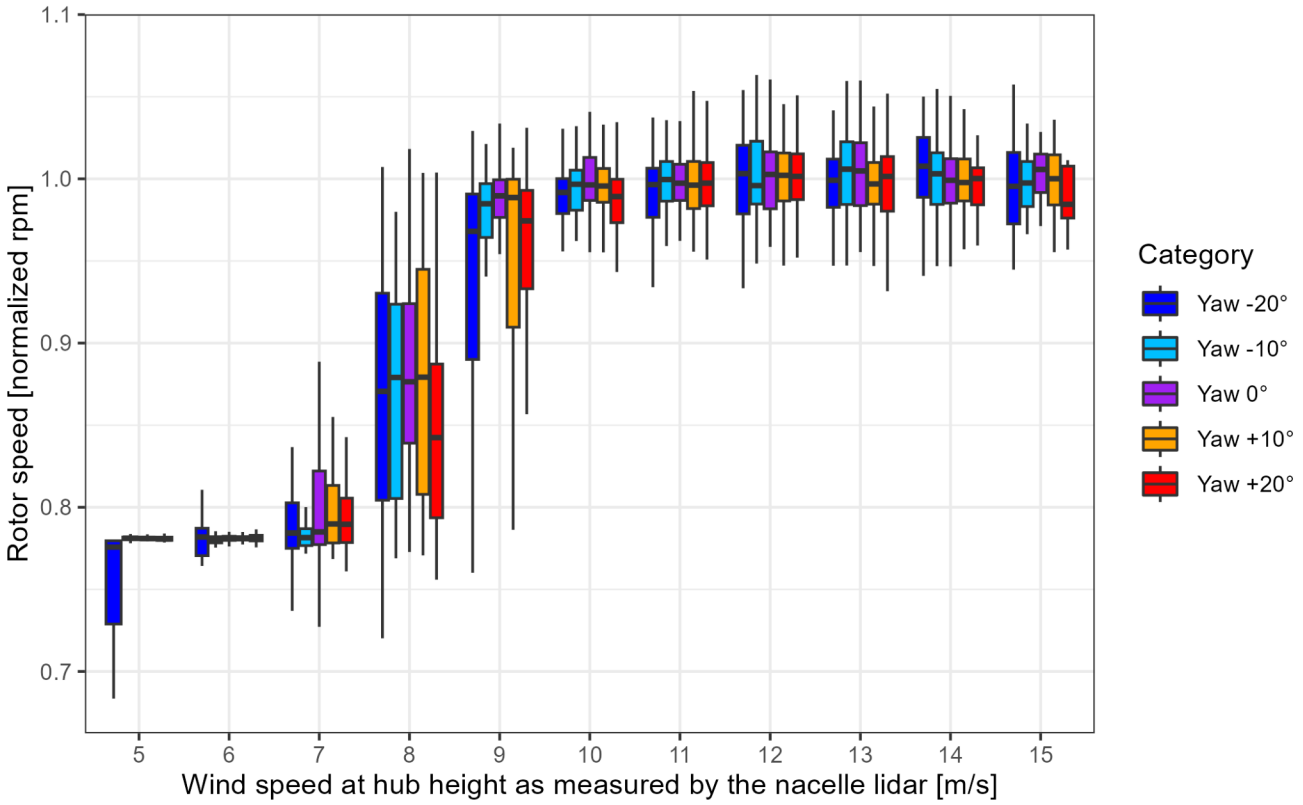

Figure 1: Rotation speed for different yaw angles. The rotor speed is normalized for confidentiality, as required by the turbine manufacturer.

sentence has been added in the manuscript to clarify this point.

3. Multiple filtering and detection parameters appear arbitrary without justification. The ±50 second rolling median window and 10 dB exceedance threshold for outlier detection (Section 3.1.2) lack supporting rationale. What is the false positive rate? How many genuine turbine noise events are erroneously filtered? Have the authors checked the manually recorded noise events against the automated event detection? The reduction of minimum samples per bin from 10 (IEC standard) to 3 (Section 3.3.2) to avoid discarding 45% of data is concerning.
Details of the parameters choice have been added in the paper. In addition, a consistency check was conducted using the field observer's notes. The observer reported 91 events over the full campaign, of which 74% resulted in a clear increase in the OASPL time series (greater than 4 dB) for SLM#1. Among these events, 54% were correctly identified by the median filter. However this test is considered of limited relevance. On the one hand, the observer may have missed some external noise events; on the other hand, some visually detected events may not be audible across all microphones and may not qualify as actual acoustic outliers. Moreover, Figures 5 and 6 of this document show that the whole procedure is relatively stable with respect to the outlier filter parameters. Regarding the reduction of the minimum number of samples per bin from 10 to 3, this is only a temporary adjustment. It is subsequently compensated for by imposing a minimum of 10 **cumulative** ***samples across microphones, per bin, relative positions, and yaw angles. A sentence has been added in section 3.3.2.***

4. The frequency-dependent nature of directivity changes (Figure 18, low-frequency effects dominate) and non-monotonic changes with wind speed (Figure 19, moderate yaw offsets produce larger changes than extreme offsets at high wind speeds) suggest complex underlying aeroacoustic physics that are not explained in the manuscript. What mechanisms separate low and high-frequency noise emission responses to yaw misalignment? Why do moderate yaw angles produce larger acoustic changes at high wind speeds? These patterns may reveal fundamental insights into trailing-edge noise, turbulent inflow interactions, or blade loading asymmetries that should be discussed at least.
A discussion has been added in section 4.2 concerning the frequency-dependent nature of directivity changes, in particular the possible influence of the yaw angle on turbulence inflow noise, whereas it is virtually ignored by turbulent boundary laryer-trailing edge noise. Concerning non-monotonic changes with wind speed, a new paired t-test was run to evaluate the hypothesis of high speed sound power levels at $\beta = -10°$ ***being higher than*** $\beta = -20°$***. The corresponding p-value being above 0.5, the non-monotonicity cannot be inferred directly from the measurements and we preferred not to interpret a statement that cannot be statistically supported.***

1.2 Detailed Comments

Section 2.1, line 95: Was any testing conducted to quantify the acoustic impact of uncut versus cut wheat? Background noise measurements (Figure 11) show up to 4 dB variation across SLMs at fixed wind speed, attributed to "local environment" differences. Quantifying the wheat crop contribution would strengthen confidence that site-specific background variations are adequately characterized rather than introducing systematic bias in turbine noise extraction.
Unfortunately, we could not conduct some tests to quantify the acoustic impact of uncut versus cut wheat. This is why we decided in the methodology to calculate a background noise for every SLM to make sure the local specifities around each of them are accounted for. We added some text in the manuscript to discuss a bit more the variations of background noise for a given wind speed.

Figures 2, 3, 6, 7: SLM identifiers should be consistent across all figures and text. Adopt a single convention (preferably the full identifier for traceability) and apply uniformly. Cross-check all figures to ensure labels match the site map.Axis labels, annotations, and colorbar text are difficult to read in several figures.
As suggested by second reviewer, we finally opted for the convention "#01". This makes it easier to read in the text and the figures. All figures were re-edited with this new convention, and we also increased the font in most of them to make them easier to read.

Section 3.2, lines 220-237: The hybrid approach introduces potential discontinuities. Report the fraction of data

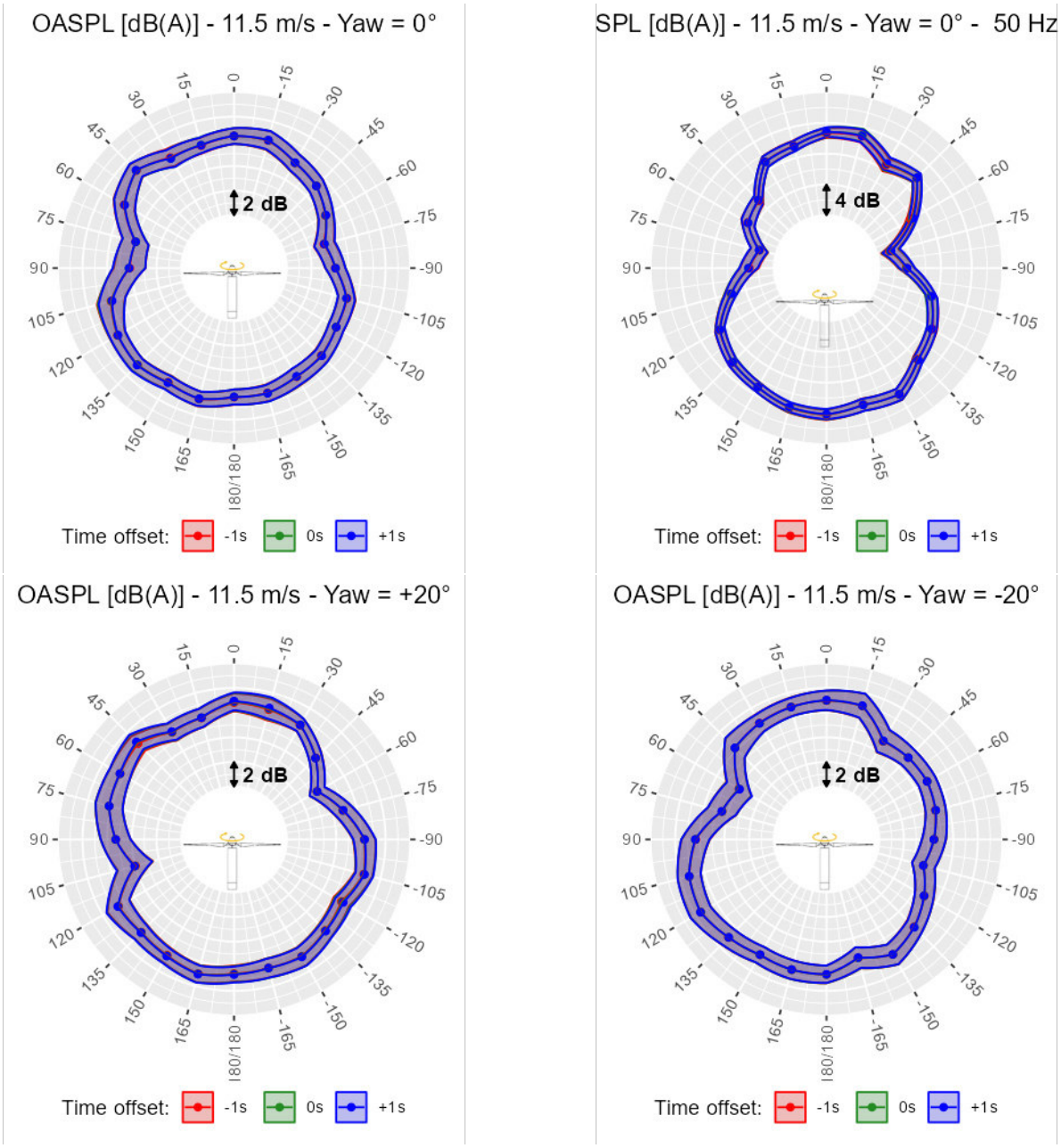

Figure 2: Results of the time offset sensitivity analysis on the directivity patterns calculated in the paper. Although only a sample of graphs are shown here, the same behavior was observed for all of them.

falling into each category and assess whether transitions between wind speed sources introduce artifacts. The 1-minute rolling average applied to nacelle lidar data may smooth out turbulence-driven acoustic fluctuations; discuss whether this temporal filtering impacts correlation between inflow conditions and noise metrics.

With the choice realized for selecting the source for the reference wind speed signal, the risk of discontinuities is much reduced. Indeed, except for the case of turbine operation under no yaw misalignment, the nacelle lidar signal is always chosen since the other sources are considered unreliable. For the 0° yaw case, there are some transitions between the inverted power curve and the nacelle anemometer sources from time to time (this happens when the turbine reaches its nominal power and the power curve cannot be inverted), but those changes are the ones that are recommended by the IEC noise standard. Finally, since we discard 3 minutes of transient data when toggling between different yaw categories, this leaves plenty of time to switch from the lidar to one of the SCADA wind speed sources. Given that the lidar is used for all yaw categories (except yaw = 0°), it is the source that is used approximately 85% of the time, while the inverted power curve and the nacelle anemometer are used only 9% and 6% of the time, respectively. These numbers and a clarification about this topic were added to the manuscript.

In order to define the best methodology for the nacelle lidar wind speed reference, we compared the correlation of different resulting signals with the reference signal coming from the inverted active power signal at yaw = 0°. This result is now presented in the Table 2 of the paper, and discussed in an additional paragraph. As can be seen, the 1-minute rolling signal is by far the one with the best correlation and show close performance with the nacelle anemometer. We therefore think that this choice limits issues in the correlation of noise metrics with inflow conditions.

Figure 16: Consider combining separate panels into a single multi-panel figure with consistent axis ranges for direct comparison. Absolute axis limits would be extremely helpful in interpreting results. If permissible, please include.

Unfortunately, we did not get the permission to show results with absolute axis limits, and we were forced to plot all graphs with relative axes only. However for this figure the two y-axes have consistent axis ranges: this can be seen thanks to the -180° curve that is common and absolutely identical in both graphs. A sentence has been added in the legend of the figure to stress this point. We prefer to keep two different sub-figures, because it makes the graphs clearer and better support the discussion in the text in which we compare the position 45°/135° and -90°/+90°, respectively.

Figure 18: Changes in directivity induced by yawed operation may be more evident if results were presented in the rotor reference frame rather than the wind reference frame. Have the authors explored this alternative representation? The strong frequency dependence (low frequencies affected, high frequencies unaffected) suggests distinct noise generation mechanisms. What aeroacoustic processes explain the frequency threshold separating responsive and non-responsive regimes? Discuss whether low-frequency changes correlate with blade loading asymmetries, inflow turbulence modulation, or wake-induced effects.

We investigated this alternative representation (see Figure 3), however the changes in directivity are not very obvious and we think it is more interesting to keep the curent representation in the wind direction frame to show the rotation of the pattern with the rotor. Also, the representation in the rotor reference frame is not ideal with the current setup, because since the yaw offsets steps are 10°, and the angular position of microphones is 15°, that forces us to resample data into 15° bins in order for the directivity patterns to be comparable.

A discussion on the effect of yaw on different aeroacoustic processes has been added in answer to question 4 above, and their relation with spectral directivity patterns. Concerning wake induced effect, we added a sentence suggesting that the observed noise increase of TI may be compensated in WFFC strategies by a reduction of turbine/wakes interactions. However, as the single test turbine was operating in free field (without wakes from upstream turbines), we do not have new material to quantify this counteracting effect. Concerning blade loading asymmetries under yaw, the blade were not equipped load sensors. Since this effect is known to be model dependent, it is difficult to correlate unknown blade loading with the noise variations we observed.

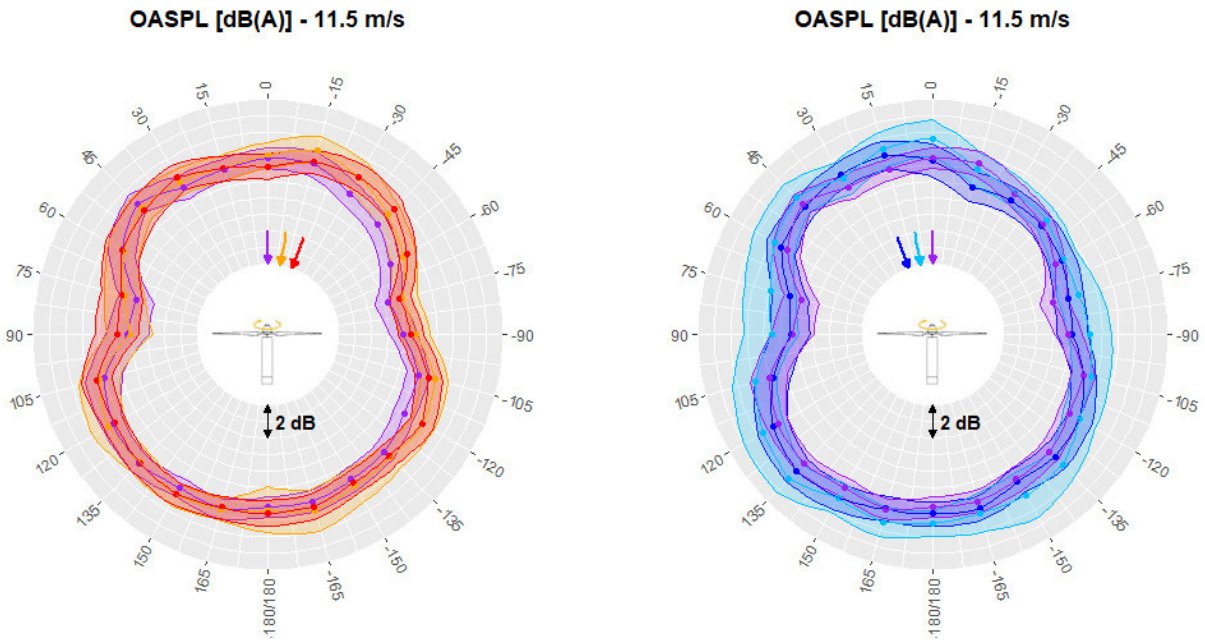

Figure 3: Sound pressure level (OASPL), displayed in the a fixed turbine reference frame. The colored arrows indicate the wind direction for each yaw misalignment case.

Figure 19: The current presentation obscures important trends. Plotting the change in noise emissions relative to the yaw 0-degree baseline as a function of wind speed would clarify how acoustic impacts vary across the operational envelope. The apparent result that moderate yaw offsets (±10 degrees) produce larger noise increases than extreme offsets (±20 degrees) at high wind speeds is counterintuitive and potentially significant. Does this non-monotonicity suggest optimal yaw angle strategies for minimizing acoustic impact while maintaining wake steering benefits? Provide mechanistic interpretation grounded in blade aerodynamics or turbulent inflow physics.
We tried plotting the turbine sound power level relatively to the flow-aligned case (see Figure 4). We find this representation is not very clear, the curves and their uncertainty bands are much superimposed. Therefore, we think it is better to keep the Figure 19 of the manuscript as is.

With this representation, it not very obvious that moderate yaw offsets (±10°) produce larger noise increases than extreme offsets (±20°) at larger wind speeds. Indeed, the -10° curve is a bit higher than the -20° curve, but its corresponding uncertainty band is also larger. The t-test run as an answer to question 4 above confirms that this difference is not statistically significant. Since there is not much difference between the +10° and +20° curves either, we prefer not to discuss these points.

1.3 Minor Edits and Technical Corrections

"Likewise" should be "Like" for grammatical correctness in this context.
Ensure consistent terminology for key concepts (e.g., "yaw misalignment" vs "yaw offset" vs "yaw control") throughout the manuscript.
Section 1, line 40: Remove extra comma in citation "(Göçmen, 2016), ."
Section 2.3, line 125: "Monday 25th" should specify "25 March 2024" for clarity, as the month is mentioned only in the preceding paragraph.

All these small corrections have been edited on the revised version of the manuscript.

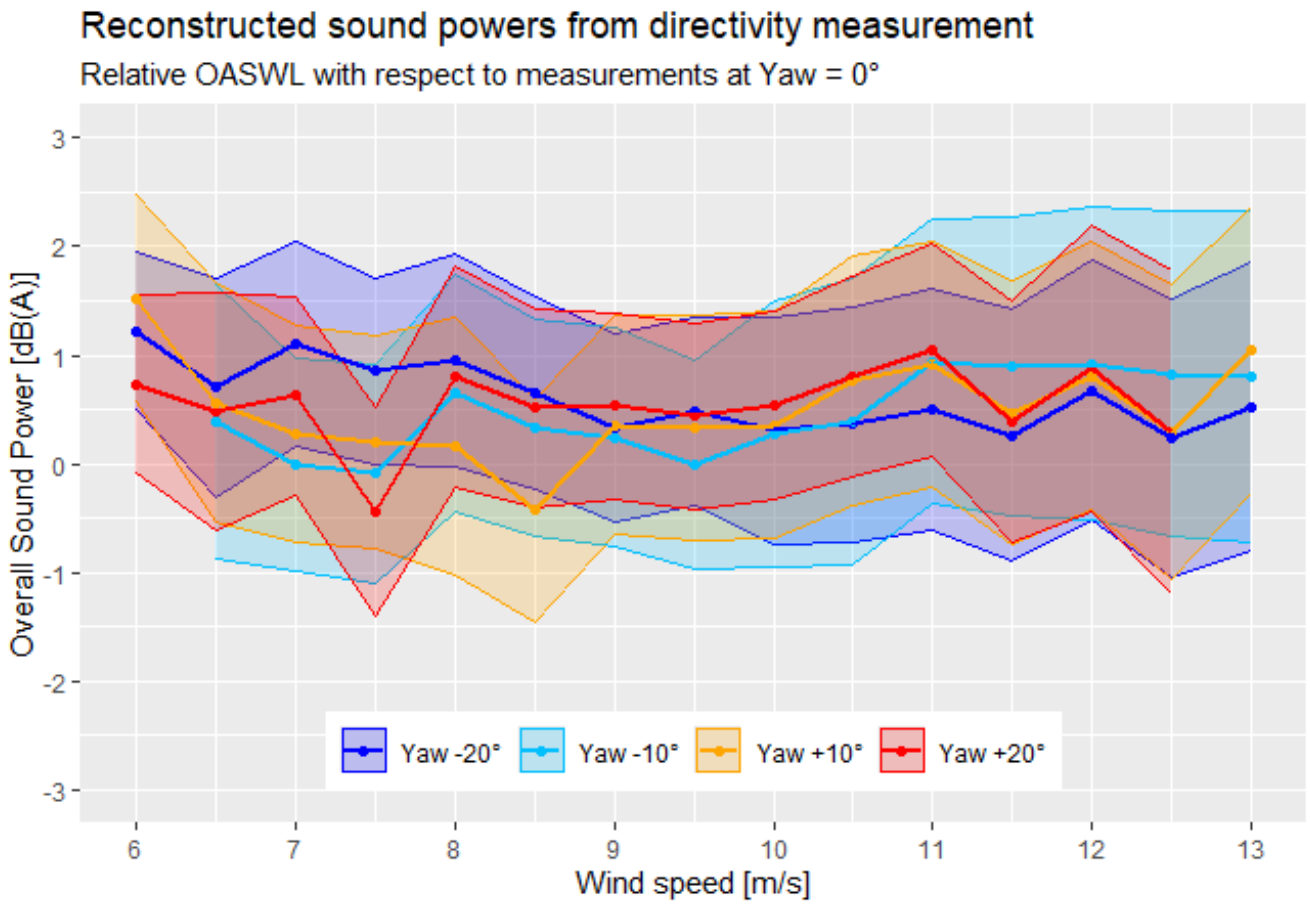

Figure 4: Relative turbine sound power level (OASWL) as a function of wind speed, with respect to measurements at Yaw = 0°.

2 Response to anonymous referee 2

In this study, the authors investigate the impact of wind turbine yaw misalignment on the noise emissions of a utility-scale onshore wind turbine. Using a circular array of 24 sound level meters (SLMs), a field campaign was conducted spanning four days that measured the acoustic impact of wind turbine operation in yaw-aligned and misaligned conditions. A nacelle-based and ground-based lidar were used to measure the wind speed, and wind speed measurements were synchronized to sound level measurements. The field measurements revealed asymmetries in noise emissions between the downstroke and upstroke sides of the wind turbine in yaw-aligned conditions, as well as between the downwind and upwind sides. In yaw-misaligned operation, a small but statistically significant increase of 0.6 dB(A) was observed, which contradicts previous studies that reported no change in noise emissions or a drop in noise emissions when a turbine is yaw misaligned. Overall, the experimental field campaign provides a useful and curated dataset to the flow control community. However, the postprocessing methodology includes several confusing decisions regarding time synchronization, wind and background sound measurements, and outlier detection. Furthermore, the main conclusions of the article contradict previous field campaigns on the same subject, with minimal discussion on possible sources of discrepancies leading to the contradictory results. Specific comments are outlined below.

Thank you very much for you thorough review of our manuscript. As you can see in our comments below, we tried to clarify our methodology with respect to the data processing and improve the discussion regarding our results and the comparison with the state of the art, hopefully improving the general quality of the paper.

2.1 Major comments

1. The primary result the authors claim is that the overall A-weighted sound power level (OASWL) of the yaw misaligned turbine is higher than its yaw-aligned counterpart, flow conditions remaining the same. However, this result contradicts that of previous studies, and the discussion regarding dicrepancies is very limited (one sentence at L449). The authors should thoroughly explore differences in their campaign that could lead to a contradictory result (distance to rotor, size of turbine, wind speed ranges, amount of data, pre/postprocessing strategy, etc.).
A section has been added at the end of the paper to discuss results reported in the literature and to propose some interpretation for the apparently diverging conclusions. In addition to this section, rotor speed curves in Figure 1 show that the curve in misaligned conditions are generally not below the $\beta = 0°$ case (except occasionnally Yaw +20°). This is a possible reason for discrepancies with the main reference of NREL.

2. Throughout several steps of the data postprocessing, it is stated that data are "visually inspected" (e.g., L115). This is also mentioned in the outlier detection (see next comment). Additional details should be provided regarding the data processing methods.
Both phrases were reformulated to provide additional details on SCADA signals considered for the visual inspection, and refer to Figure 8 for the case of a noisy event.

3. The outlier detection uses a threshold value of 10 dB to filter out observations relative to a ±50-second running median. However, figure 10 showcases the deficiency here: one spike in SPL (around 21:14) is removed as an outlier, but a very similar looking spike around 21:42 is not removed. What is the sensitivity of the results to the outlier removal strategy? How do the results change if other values for the running median window and/or dB threshold are modified? And how were the values in the study selected?
We added in the paper a justification of the selection procedure for the outlier detection in section 3.1.2. A sensitivity analysis to outlier detection has been conducted using a much more sensitive filter with a threshold value of 5 dB to filter out observations relative to a ±25-second running median, with a safety window of ±20 s. The total number of outlier events raised from 2150 to 4616. Sound level changes are very limited as can be seen on the directivity patterns on Figure 5. Minimal variations are observed as well concerning the estimated sound power levels on Figure 6. The mean absolute variation stays below 0.04 dB between the two filters. Other parameter values have been

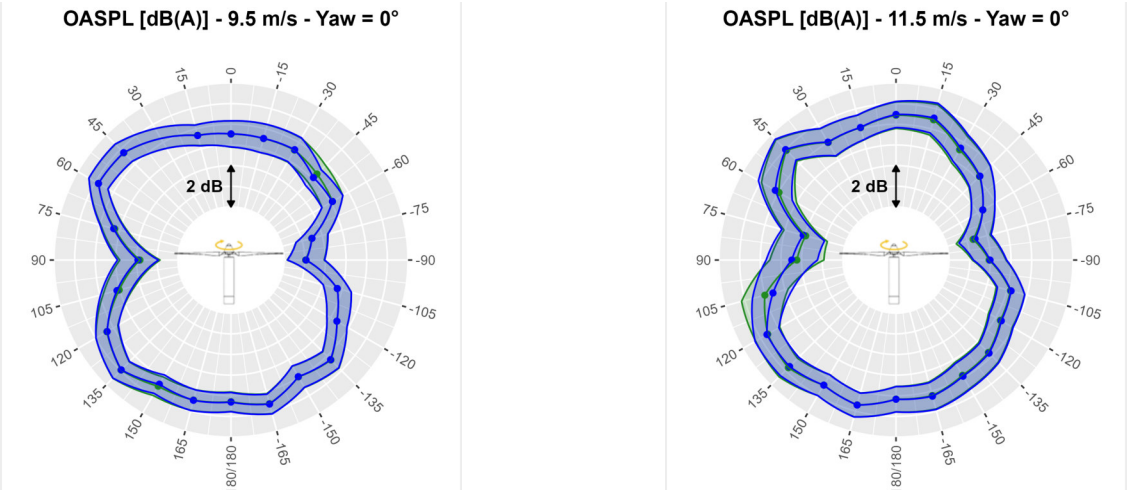

Figure 5: Sensitivity of directivity patterns to outlier filter. The filter used in the paper (with a level threshold at 10 dB, from a ±50 second running median, with a safety window of ±20 s) is compared to a more restrictive filter with a level threshold at 5 dB from a ±25 second running median with a safety window of ±20 s.

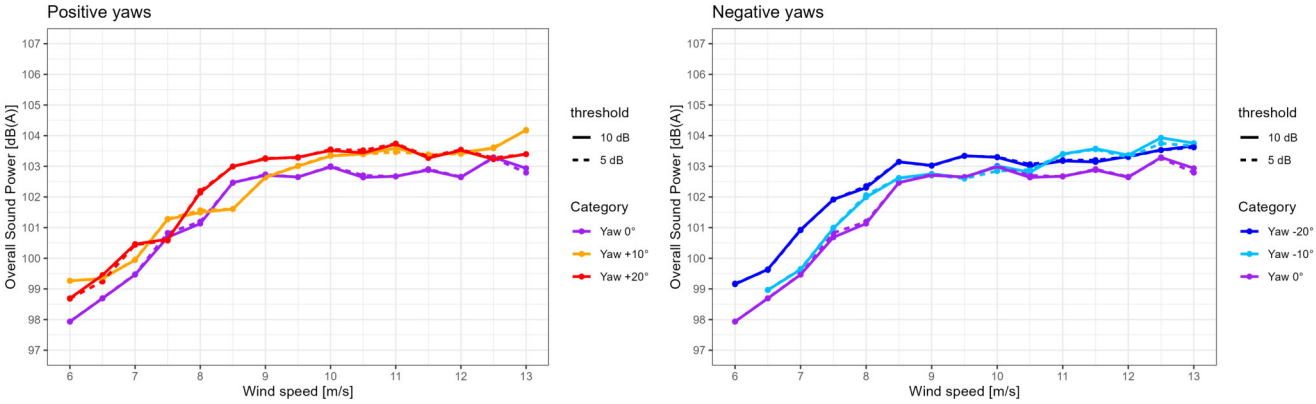

Figure 6: Sensitivity of estimated sound power levels to outlier filter. The parameters are identical to Fig.5

tested provided the same order of magnitude.

4. The study would benefit from a specific discussion regarding the measurement of the freestream wind speed. For example, what is meant by "the resulting wind speed signal [from the ground-based lidar] was too noisy and did not correlate well with the SCADA data"? Typically, SCADA data are output in 10-minute frequencies, however the study here seems to aim at 10-second time intervals. Do the various methods agree well in yaw-aligned flow, or when the background noise measurements are active? If not, then that would raise concerns for using different measurement channels throughout different experiments (yaw-misaligned vs yaw-aligned vs off).
Truly, SCADA data are typically output in 10-minute resolution, however the application if the IEC 61400-11 standard requires the recording of SCADA data at 1-second frequency and aggregation of these data into 10-second chunks. We therefore had to process lidar data into 10-second chunks as well in order to be able to associate them with the SCADA and acoustics data. Several methods were developed for that objective, and compared to the active power reference signal in yaw-aligned flow. We cannot use the background measurement periods for this kind of comparison : indeed, since the active power is null the power curve cannot be inverted, and as pointed out in the IEC noise standard the nacelle anemometer measurement is likely to be biased when the turbine is stopped. The Table 2 in the manuscript now recaps the correlation between the different available lidar wind

speed signals: it can be seen that the one chosen for the study is the best performing by far. A new paragraph has been added to discuss those results.

5. Section 3.3.1: Is wide variation in SLM background noise physical, or could be due to calibration error in the SLM? If it is physical, then this suggests there are much larger variations (upwards of 4 dB) in small variations in location around the wind turbine (¡100 m), compared with relatively small differences (order 0.5 dB(A)) in noise due to asymmetries and yaw misalignment.
The SLMs were calibrated every day before the measurements begin and did not show any inconsistencies during the 4 days of measurement (except for the case of SLM #06 that is mentioned in Section 3.1.3). We therefore think the wide variation in SLM background noise is rather physical. There is indeed much larger variations in due to the location of the SLM compared to the effect of yaw misalignment, however since we calculated in the methodology a specific background noise for each location, we expect that these variations cancels out when we derive the turbine specific noise. We added some text in the manuscript to discuss a bit more these variations of background noise and justify our choice for a specific background noise calculation by SLM.

2.2 Points comments

1. Figure 1: As I understand it, this decision matrix describes acoustic curtailment for a specific four-turbine wind farm. How general is this decision matrix? Additionally, the times of curtailment center in the evening and nighttime hours, while this experiment is performed only during daytime hours. How might that affect the results or conclusions?
The lookup table presented in Figure 1 is not the one that is implemented at the farm. It displays a very typical case of acoustics curtailment in France, since they are generally defined according to Daytime/Nighttime, wind sector, wind speed and season of year. This is done to account for specifities of the site both in terms of climatology (e.g. long-term wind rose), acoustics propagation, local regulatory constraints and background noise observed at the location of people habitation (i.e. a few hundred of meters away from the turbine). The measurements that we describe in this manuscript follows the procedure described in the standard IEC 61400-11 and are realized in the close vicinity of the turbine in order to characterize its specific noise only, independently of all those aspects. Therefore, the fact that our measurements were realized during the day, and curtailment in France generally applied during the night does not change our conclusions. Of course, any knowledge gained thanks to this measurement could in turn be used to update some inputs of the modeling toolchain that is used to optimize our acoustics curtailment, but this will be the subject of future work (some of it will be realized in the scope of TWAIN project).

2. L94: the terrain inclination varies between 29° and 31.5°. Perhaps I am misunderstanding how inclination angle is computed, but this does not seem "very simple and flat". Clarity would be appreciated.
This sentence refer to the terrain inclination angle ϕ defined by the IEC 61400-11 standard (see the figure 4 of the standard) as :

$$\phi = arctan\left(\frac{HH + dz}{HH + D/2}\right) \tag{1}$$

where HH is the turbine hub-height, D the turbine diameter, and dz the difference in altitude between the turbine and the SLM location. For a perfectly flat terrain ($dz = 0$ m) and the corresponding turbine dimensions ($HH = 80$ m and $D = 110$ m, this would yield $\phi = 30.65°$). Therefore with ϕ varying between 29 and 31.5° depending on the SLM location, we are close to be in the ideal case of the flat terrain. The phrase in the manuscript has been reformulated to clarify how ϕ is defined.

3. L126: It may be worth noting that high windspeed events (i.e., above-rated conditions) and high turbulence conditions are less important to WFFC applications. What were the wind speeds during this period of no testing?
This is a good point, we added a sentence in the manuscript to point that out. The wind speeds when

we were forced to stop the 6^{th} round of measurement were above 15 m/s.

4. Figure 4: How is vertical shear computed?
The wind shear is estimated by fitting a power law to 14 planes of measurement ranging from 40 to 140 m (i.e. the span of the turbine rotor). This clarification has been added in the manuscript.

5. Figures 6-7 may be combined into one figure to save space. Furthermore, the names of the SLMs should be changed in figure 7 and throughout (e.g., figure 8) to more useful names (such as "SLM #XX" as used throughout the text).
Figures 6 and 7 are one-column figures, in the discussion manuscript that leaves a lot of blank space but in the final version (two column display) they will end up side by side. All figures have been reedited to harmonize the SLMs names in all of them.

6. Regarding the clock drift correction, what is the point of steps 1-3 (section 3.1.1), when step 4 seems to align all of the time signals with the turbine operation/SCADA clock?
By considering first all microphones for estimating the clock drift correction, we calculate a time offset which is based on multiple pairs of microphones and that can therefore be considered more robust and if it were just obtained though a direct comparison to a single SCADA signal. A sentence has been added in the manuscript to clarify this point.

7. L212: Was the dB offset correction to SLM #06 calculated during turbine operation, or only during background noise measurement periods? If the offset correction was computed for the entire time history, then it seems like that could bias the results.
The offset correction was calculated for this entire time history. This could indeed bias the result. We decided to discard the data of SLM #06 for the first measurement day and updated all the figures in the paper. The impact of this change is negligible and does not change at all the mains conclusions of this research.

8. L251-254: Please clarify the method for measuring wind direction at hub height. What "external sensors" are referred to in L253? What averaging or interpolation methods (if any) are used to measure the hub height wind direction with the ground based lidar?
The two external sensors considered here are the nacelle-mounted and the ground-based lidars. The 10-minute wind direction signal, averaged over all planes of measurement of the ground-based lidar is taken as reference for the wind direction. This precision has been added to the manuscript.

9. Table 3: The yaw angle uncertainty/error is missing from the sources of error. Previous field campaigns (e.g., McKay et al., Wind Energy (2013)) have noted significant discrepancies in turbine alignment from the incident wind, due to slow-reacting controllers and turbulence.
This is a good remark. There is indeed an additional source of uncertainty due to the wind dynamics and slow reaction of the turbine yaw controller to changing wind direction. However, our dataprocessing is based on the recommendations of the IEC 61400-11 standard, which does not consider this source of uncertainty and since we did not have the means to estimate it accurately we decided to keep the same categories as the ones listed in the standard. A comment and a reference to this citation have been added in the manuscript with respect to this point.

10. For this audience, it would be useful to have a brief discussion clarifying between OASPL (pressure levels) and OASWL (power levels). Why is OASPL shown in figures 14-18 but then OASWL shown in figure 19?
An explanation of the difference between SPL and SWL has been added in section 3.3.3, together with a clarification of the term **overall**. ***OASPL is shown in figures 14-18 because they show local values (noise levels measured at each microphone positions), while figure 19 show integrated values over all microphone positions. OASWL estimates the global acoustic energy flux radiated by the turbine in all directions at once.***

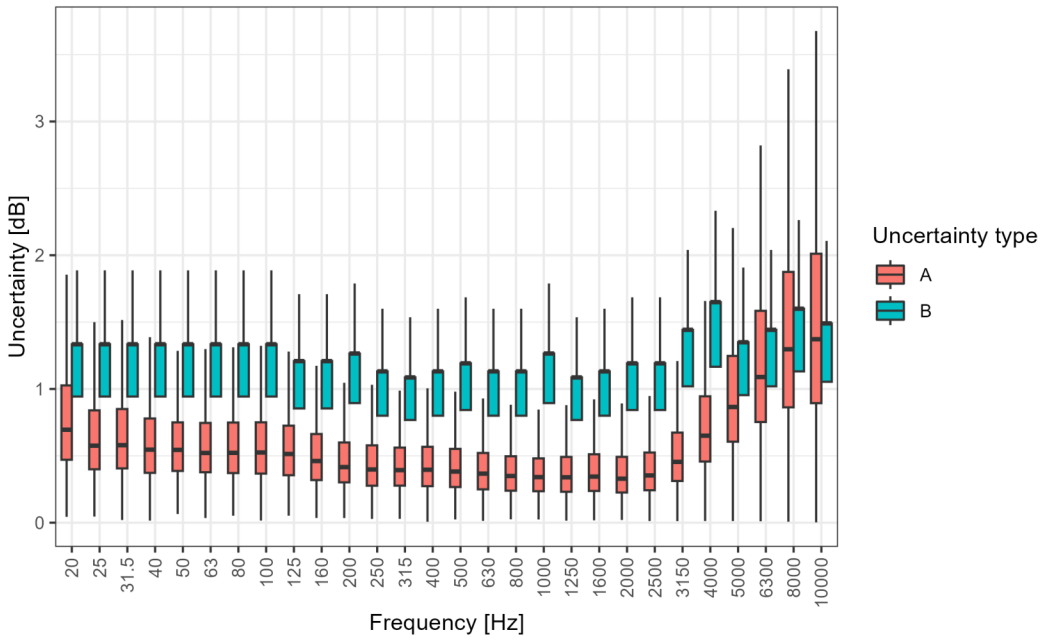

Figure 7: Uncertainty type statistics for total noise as a function of 1/3-octave frequency bands. Type A is related to the statistical dispersion of measured data while type B is related to estimated uncertainties of material and instrumentation.

11. L383-384: How does the discussion of airfoil camber/asymmetry relate to the data collected in this experiment and/or this wind turbine model?
The discussion on camber has been completed to finalize the reasoning on directivity pattern asymetry. We do not have the detail of the blade geometry so the discussion stays on a general level, without quantitative assessment from this specifc experiment.

12. L394-395: where does the increased uncertainty at higher frequencies come from? As I understand it, the uncertainties in table 3 are all constant with frequency/octave band.
Concerning table 3, u_{B2} ***and*** u_{B4} ***are frequency dependant so "Type B" uncertainty at 5 kHz is indeed higher than at 500 kHz. This can be observed in Figure 7. However the main variation in uncertainties across the frequency range is provided by "Type A" contributions, related to the natural variation of sound levels. A sentence has been added in section 4.1.***

13. Figure 19 and surrounding text: the uncertainty bars overlap significantly, yet the p-value is small. Why is this?
This is because the p-value is an aggregated indicator of the whole curve, over all windspeed bins. Uncertainty bars only refer to a specific wind speed bin. A p-value < 0.05 ***indicates that it is highly unlikely that all these points at*** $\beta = 0°$ ***lie below the other curves due solely to uncertainty (as quantified by the error bars).***

2.3 Minutiae/typos

1. L24: A citation to Meyers et al. Wind Energy Sci. (2022) would be particularly relevant here.
Very good point, we added the citation.

2. L51 and throughout: what does TWAIN stand for? Is it an acronym?
TWAIN is the short name for Integrated, Value-based, and Multi-objective Wind Farm Control pow-

ered by Artificial Intelligence. Since the project name is quite long, and the acronym for TWAIN not obvious, we did not detail in the manuscript the full project name but instead just added a link to the project website in the references.

3. L89, L104, and throughout: some writing is too informal for an academic publication.
These sentences and a few other in the manuscript have been reformulated.

4. L144: Please be more specific than "Unfortunately some sensor defaults introduced a loss on data in some conditions."; this sentence (and others like it in the manuscript) should be omitted.
This sentence have been rephrased.

5. Figure 5 caption and elsewhere (L155, L276): "10-seconds sample" → "10-second sample".
These typos have been corrected.

6. The opening paragraph in section 3 is fully described in figure 12; consider moving figure 12 earlier and rephrasing the intro text in section 3.
Thanks for the suggestion. Indeed, it makes more sense to move the figure in the intro of section since this also how it is done in the standard. The text have been rephrased accordingly.

7. L301: to clarify, is the OASPL also binned on wind speed, in addition to relative position and yaw angle?
The mention to wind speed has been added.

8. Figure 16, y-axis: "OAPSL" → "OASPL"
The typo has been corrected.

9. L472: The acronym SWL is never used in this manuscript.
This unused acronym as been removed.

10. L476: "first of his kind" → "first of its kind"
11. L476: "WFC" → "WFFC"
Both typos have been corrected.

Experimental investigation of the effect of wake steering on the noise emission of a commercial wind turbine

Thomas Duc[1,*] and Arthur Finez[1,*]

[1]ENGIE Green France, 6 rue Alexander Fleming, 69007 LYON, FRANCE
[*]These authors contributed equally to this work.

Correspondence: Thomas Duc (thomas.duc@engie.com) and Arthur Finez (arthur.finez@engie.com)

Abstract. Wake steering is a wind farm flow control (WFFC) strategy that involves intentionally misaligning the most upstream wind turbines to deviate their wakes away from the downstream wind turbines. This study investigates the acoustic implications of such a strategy. A novel acoustic setup ~~was~~ is implemented, involving 24 ground-based sound level meters arranged on a circle around an industrial 2.2 MW wind turbine, positioned at tip-height distance. This configuration enables a fine angular resolution of 15°. Incoming wind conditions ~~were~~ are monitored using both a nacelle-mounted plus a ground-based lidar. A test protocol closely aligned with IEC 61400-11-1 ~~was~~ is followed to characterize the turbine's noise emissions under various yaw ~~offset~~ misalignment settings, ranging from -20° to +20° across a broad spectrum of flow conditions. A dedicated data cleaning and analysis procedure ~~was~~ is developed to derive ground-level turbine noise directivity patterns. In the absence of yaw misalignment, the directivity patterns exhibit the typical two-lobe structure. However, slight but statistically significant asymmetries ~~were~~ are also observed: the downstroke side ~~was~~ is in average 0.6 dB(A) louder than the upstroke side, and the downwind side ~~was~~ is 0.4 dB(A) louder than the upwind side. These specificities are not captured by most of the analytical models used by the profession. When yaw ~~control was~~ misalignment is applied, a modest increase of approximately 0.6 dB(A) ~~was~~ is observed in the estimated overall sound power level. The results from this innovative experiment confirm the fact that operators must consider other metrics than just power production when implementing WFFC on their projects, and that more advanced noise models are required for the development of a framework allowing multi-objective WFFC.

1 Introduction and context

Wind Farm Flow Control (WFFC) is a concept in which turbines within a wind farm are controlled in a coordinate way to accomplish a common objective, such as increase in farm power production, reduction in turbine loading, or active power control (Boersma et al., 2017). Two strategies are generally considered to achieve these goals : the axial induction strategy in which the upstream turbines are down-regulated to leave more kinetic energy for the downstream turbines and the wake steering strategy that consists in intentionally misaligning the upstream turbines to deflect the wake away from the downstream turbines. For both of them, the performance of the most upstream turbines is reduced so that the one of the downstream turbines is improved: the WFFC is successful when the downstream gain is compensating for the upstream loss and the overall power production is increased. WFFC has been an intense subject of research over the past decade with many full scale experiments

organized all over the world on commercial wind farms (Meyers et al., 2022). The vast majority of these experiments were focused on the objective of improving the total energy production of a wind farm, while only a few of them tackled the issue of load reduction (Damiani et al., 2018; Dana et al., 2022) or active power control (Göçmen, 2016),.

Among the two strategies, wake steering is the one that has shown the higher potential for power improvements, with a track record of many full scale field tests showing significant energy gains (see e.g. Fleming et al. (2017, 2019, 2020, 2021); Simley et al. (2021); Doekemeijer et al. (2021); Howland et al. (2022)). On the other hand, meaningful power gains seems more difficult to achieve through axial induction control, although a few full scale experiments were able to highlight performance improvements for specific wind sectors (van der Hoek et al., 2019; Bossanyi and Ruisi, 2021). When averaging over the full wind rose to get the total annual energy gains, those gains are drastically reduced and consequently this strategy might be more suitable for achieving load reduction and active power control (Boersma et al., 2017).

Another less widespread objective that can be achieved through WFFC is acoustic control of a wind farm (Nyborg et al., 2023). Wind turbines are controlled together to comply with the local legislation and make sure the total noise emissions of the farm remains below a given threshold, while trying to maximize the total energy production. This is usually accomplished using an axial induction strategy during which specific noise reduced operation (NRO) modes are activated according to a list of criteria (for instance time of day, period of year, incoming wind speed and direction sector). A practical example of an implemented acoustic curtailment plan is presented in Figure 1. Note that it is usually defined using numerical simulations and simple noise source models assuming omnidirectional noise sources. A variation of ± 0.5 dB(A) in the source power definition can be qualified as "small" from the acceptance point of view, since it is lower than 1 dB, the level variation threshold of human hearing. However, in critical situations, such variation can lead to significant changes in the curtailment plan associated with variations in Annual Energy Production (AEP) of the order of 1%, since the chosen curtailment plan must strictly comply with local noise regulations.

An expert elicitation about WFFC realized a few years ago only ranked the noise reduction objective in second to last position (van Wingerden et al., 2020). However, in some countries where regulations and constraints are very restrictive, the topic of farm noise emissions has become increasingly important. As an example, the large majority of newly developed wind projects in France are now concerned with an acoustic curtailment, leading to an average 2.8% reduction in AEP (Willis, 2023).

The TWAIN research project (TWAIN, 2023) aims at providing a framework for multi-objective WFFC: increase in power production, reduction in turbine loading, complying with grid requirements or environmental regulations (acoustics, wildlife and social consciousness). Therefore, understanding the impact of WFFC actions not only on turbine power and loads but also on other aspects such as farm noise emissions is critical to design the optimal strategies to be applied by the wind farm owner or operator. In that scope, acoustic models must be improved and validated to bridge the gap with the current state of the art.

Noise impact studies dedicated to the permitting of industrial wind farm projects most often involve omnidirectional point noise sources located at the nacelle center of the wind turbines. However, several scientific studies challenge this omnidirectionality assumption. Acoustic measurements on full scale wind turbines consistently show a "noise dip" of a few decibels in the rotor plane (Oerlemans and Schepers, 2009; Buck et al., 2016; Okada et al., 2016), which is generally reproduced by more

Time of day	Wind sector	Season	Turbine	Wind speed												
				3 m/s	4 m/s	5 m/s	6 m/s	7 m/s	8 m/s	9 m/s	10 m/s	11 m/s	12 m/s	13 m/s	14 m/s	15 m/s
Night	North-East	Spring & Summer	WT1	Mode 0	Mode 0	Mode 0	Mode 2	Mode 2	Mode 2	Mode 2	Mode 2	Mode 2	Mode 2	Mode 2	Mode 2	Mode 0
			WT2	Mode 0	Mode 0	Mode 0	Mode 0	Mode 1	Mode 1	Mode 0	Mode 0	Mode 0	Mode 0	Mode 0	Mode 0	Mode 0
			WT3	Mode 0	Mode 0	Mode 0	Mode 2	STOP	STOP	Mode 1	Mode 1	Mode 0	Mode 0	Mode 0	Mode 0	Mode 0
			WT4	Mode 0	Mode 0	Mode 0	Mode 2	Mode 2	Mode 2	Mode 0	Mode 0	Mode 0	Mode 0	Mode 0	Mode 0	Mode 0
		Fall & Winter	WT1	Mode 0	Mode 0	Mode 0	Mode 0	Mode 4	STOP	STOP	Mode 4	Mode 0	Mode 0	Mode 0	Mode 0	Mode 0
			WT2	Mode 0	Mode 0	Mode 0	Mode 0	Mode 4	STOP	STOP	STOP	Mode 0	Mode 0	Mode 0	Mode 0	Mode 0
			WT3	Mode 0	Mode 0	Mode 0	Mode 2	Mode 2	Mode 4	Mode 4	Mode 4	Mode 0	Mode 0	Mode 0	Mode 0	Mode 0
			WT4	Mode 0	Mode 0	Mode 0	Mode 2	STOP	STOP	Mode 4	Mode 4	Mode 0	Mode 0	Mode 0	Mode 0	Mode 0
	South-West	Spring & Summer	WT1	Mode 0	Mode 0	Mode 0	Mode 0	Mode 0	Mode 0	Mode 0	Mode 0	Mode 0	Mode 0	Mode 0	Mode 0	Mode 0
			WT2	STOP	STOP	STOP	STOP	STOP	STOP	Mode 2	Mode 2	Mode 2	Mode 2	Mode 2	Mode 2	Mode 2
			WT3	Mode 0	Mode 0	Mode 0	Mode 0	Mode 0	Mode 0	Mode 1	Mode 1	Mode 1	Mode 0	Mode 0	Mode 0	Mode 0
			WT4	Mode 0	Mode 2	Mode 2	Mode 2	Mode 2	Mode 2	Mode 2	Mode 2	Mode 2	Mode 2	Mode 2	Mode 2	Mode 2
		Fall & Winter	WT1	Mode 0	Mode 0	Mode 0	Mode 2	Mode 2	Mode 4	Mode 4	Mode 2	Mode 2	Mode 2	Mode 2	Mode 0	Mode 0
			WT2	Mode 0	Mode 0	Mode 0	STOP	STOP	STOP	Mode 4	Mode 4	Mode 2	Mode 2	Mode 2	Mode 0	Mode 0
			WT3	Mode 0	Mode 0	Mode 0	Mode 0	Mode 0	Mode 0	Mode 0	Mode 0	Mode 0	Mode 0	Mode 0	Mode 0	Mode 0
			WT4	Mode 0	Mode 0	Mode 0	Mode 2	Mode 2	Mode 2	Mode 2	Mode 2	Mode 2	Mode 1	Mode 1	Mode 0	Mode 0

Figure 1. Typical acoustic curtailment applied in a wind farm. The wind farm control is applied as a look-up table giving the NRO mode to be followed by each turbine as a function of several environmental criteria. The turbines are supposed to be operated in full power mode outside the conditions provided in this lookup table (e.g. during daytime).

advanced analytical models. On the contrary, complex multi-lobe structures as well as upwind/downwind and upstroke/downstroke asymetries are observed but not fully captured by those models.

Similarly, while axial induction control has been used for years to implement acoustic curtailment plan, the effect of wake steering on noise emissions remains an open question. Only two full scale experiments related to this topic were found in the literature, with one pointing toward a reduction of the noise emission due to the application of yaw misalignment (Hamilton et al., 2021) and the other showing no hearable impact (Bonsma et al., 2019). Since wake steering has already demonstrated positive energy gains and begins to be deployed on many wind farms (Harrison et al., 2025), there is a need to quantify more accurately its consequences on acoustics.

This paper introduces a novel field campaign designed specifically to study the effect of turbine yaw ~~control~~ misalignment on sound magnitude and directivity. A commercial wind turbine has been fully surrounded by 24 ~~microphones~~ sound level meters (SLM) in order to measure with a high resolution the directivity pattern of its noise emissions and track how it is changed when yaw misalignment is applied. In the following the term "directivity" refers to the ground trace of the horizontal noise directivity, as measured by a circle of ~~microphones~~ SLMs around the turbine.

The field campaign, described in Sect. 2, was prepared following the recommendations of the IEC 61400-11-1standard as close as possible (IEC, 2012), and therefore terms and notations adopted in this article are mostly inspired from this reference. However, due to the extensivity of the setup, ~~some~~ a few adjustments to the standard procedure had to be applied. Those are detailed in Sect. 3 along with the methodology applied to process the large dataset recorded during the campaign. Section 4

provides the analysis of noise directivity pattern and effect of yaw misalignment. The goal of this experiment is to provide a high quality dataset that can be used within the TWAIN project to improve acoustics models; Sect. 5 will thus conclude this paper and offer perspectives about future developments realized in the scope of the project.

2 Description of the field campaign

The field campaign was realized from 25 to 28 March 2024 on a commercial wind turbine (diameter D = 110 m, nominal power P = 2.2 MW and hub height HH = 80 m) in a farm operated by ENGIE Green and located in the northern region of France. This section gives a summary of the experimental setup, the procedure followed and the wind conditions recorded during the test.

2.1 Experimental setup

Figure 2 recaps the experimental setup that was implemented for the campaign. The 24 sound level meters (SLM) surrounding the turbine were located every 15° at a distance of approximately one turbine tip height (135 m) from the turbine. Distance to the tower base was measured ~~thanks to~~ using a laser pointer and ~~cross checked using their GPS position: the values obtained for laser measurement~~ verified by comparing the GPS coordinates of the turbines and each SLM. The obtained values ranged from 132.5 m to 139.4 m which ~~fulfills~~ is consistent the $\pm$ 20%, $\pm$ 30 m tolerance criteria of the IEC standard (IEC, 2012). Angular difference between two successive SLM was evaluated using their GPS coordinates and varied from 11.6° to 18.2°. The distance from the ground-based Windcube lidar to the turbine was also estimated based on its GPS coordinates and found to be roughly 330 m.

The site is very simple and flat, and the calculated terrain inclination angle ϕ ~~for all SLM position~~ (defined in the standard with the line joining the SLM and the turbine hub) for all positions varied between 29° and 31.5°, well within the 25° - 40° ~~range preconized by the IEC standard~~preconized range. The surrounding terrain mostly consists of wheat crops. In late March, at the time of the experiment, those crops were reaching a height of about 30 cm. In order to prevent any disturbance from the noise caused by the wind on those crops, they were cut for a diameter of roughly 3 m around each SLM position. The Fig. 3 shows one SLM together with controlled turbine in the background.

SCADA data for the misaligned turbine was collected during the test at 1 second resolution for the most important variables: active power, wind speed, vane angle, nacelle position, rotor and generator speed, pitch angle. Almost all acoustics sensors were removed each night and reinstalled every morning at the same location. They were checked for time synchronization and calibration before new measurements were launched. Both the overall sound pressure levels and 1/3-octave bands spectra were recorded with a sampling period of 1 second. ~~Measurements from lidars were also done with the same~~ Lidar measurements were acquired at an identical temporal resolution.

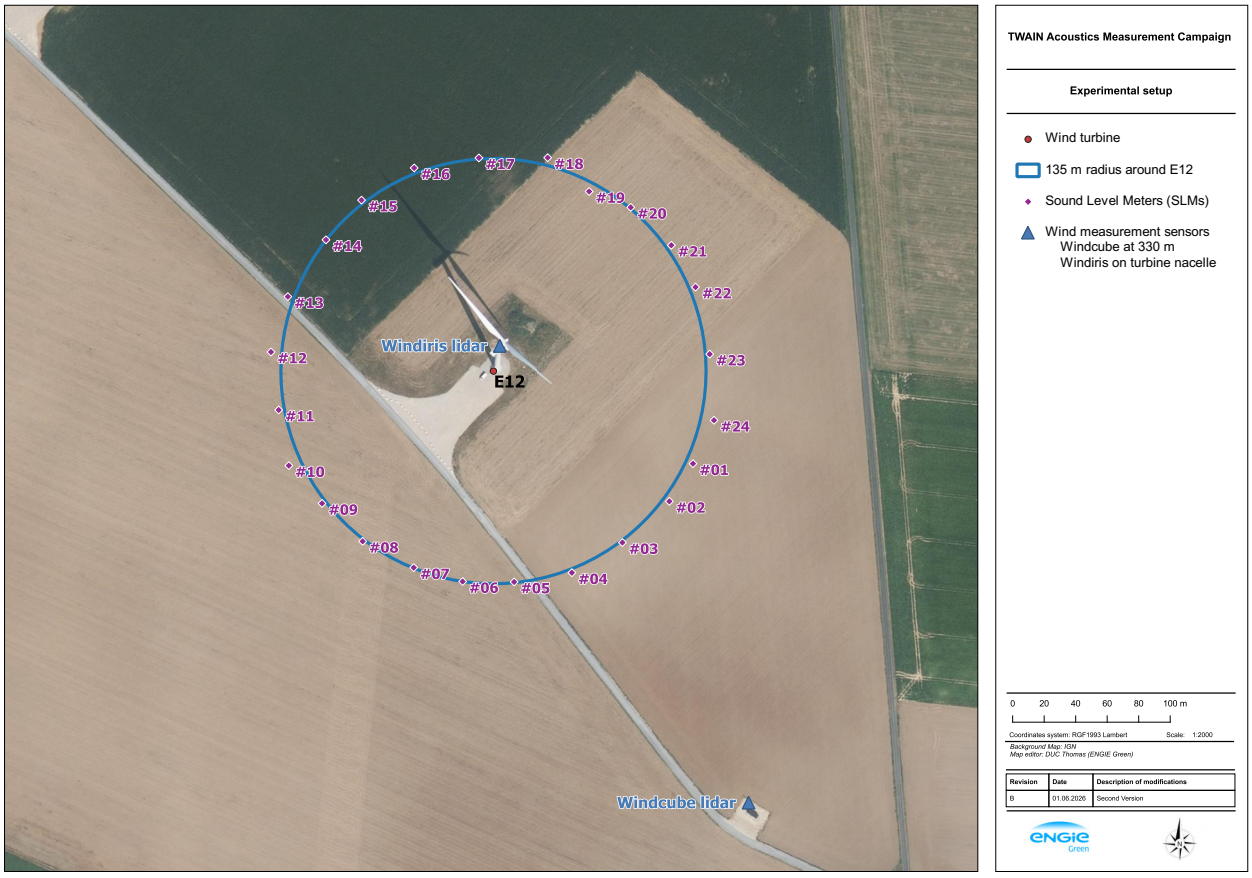

Figure 2. Experimental setup of the TWAIN acoustic measurement campaign. External wind sensors include a the ground-based Windcube lidar located at 330 m from the turbine and a nacelle-mounted Windiris lidar. The 24 ~~microphones~~ sound level meters were placed approximately 1 total height of the turbine (135 m) from the tower base

2.2 Test procedure

In order to study the effect of yaw misalignment on wind turbine noise in similar atmospheric conditions, a specific measurement routine was designed for the campaign. The yaw set point parameter β is defined as the angle between the nacelle axis and the incoming main flow direction.The turbine was sequentially yawed from β = -20° to β = +20° by step of 10°, staying in each position for 40 minutes. Between two successive positions, background noise and turbine noise measurements were also conducted with β = 0°, each of them lasting 10 minutes. Finally, a period of 3 minutes was considered for each transition to give some time for the turbine to move or restart and let the flow reach its equilibrium for the new position. The full routine, planned to last almost 4.5 hours can be found in Tab. 1.

Figure 3. Picture of one SLM with E12 wind turbine in the background. The wheat crops around the SLM were cut to prevent noise disturbance. Following the recommendations of the IEC standard (IEC, 2012), all ~~microphones~~ SLMs are installed on a woodboard of 1 m diameter and covered by two windscreens.

In practice, this routine could not be programmed in the control software and the turbine was manually switched between each state by an operator. The periods in each position were thus approximately followed but were maintained at least as long as indicated above. Overall, the fulfillment of one full round of measurement lasted ~~a bit~~ slightly longer than originally planned. During the data post-processing, the SCADA 1 second timeseries ~~was~~ of active power and nacelle position were visually inspected to ~~identify precisely the moments~~ mark precisely the exact timestamps of switching from one phase to another. In operation phases, the target turbine was settled to the full power mode, i.e. without any NRO mode implemented.

The two nearest turbines in the farm (WT10 and WT11 located at respectively 345 and 770 m at the North-West of WT12) were shut down at the beginning of each round of measurement and maintained stopped for the full duration of the test to avoid disturbing the test and record data with a satisfactory signal to noise ratio. The closest neighboring turbine still in operation was located more than 1 km away. A person was also constantly present on site to keep a track record of the noisy events (such as a plane or car passing by) so that they could be properly considered and filtered afterwards.

2.3 Wind conditions recorded during the test

The experiment consisted of 6 rounds of measurements that were conducted over the 4 days : one on ~~Monday~~ 25 ~~th and on Tuesday~~ March 2024 and on 26 ~~th~~March 2024, and two on ~~Wednesday~~ 27 ~~th and Thursday~~ March 2024 and 28 ~~th.~~ March 2024. Round 2, 4 and 6 could not be realized completely due to the appearance of rain in the afternoon of the 26th and 27th and of

Table 1. Description of the measurement routine followed during the test. Each phase is planned to last 40 minutes, the background noise and turbine noise measurement at $\beta = 0°$ are spread in 4 steps of 10 minutes each to be recorded closer to the misaligned conditions.

Phase	Yaw ~~offset~~ misalignment β (°)	WT operation	Duration
Turbine noise measurement	-20	Operating	00:40:00
Background noise measurement	-20	Stopped	00:10:00
Transition	Toggling -20 -> 0	Starting	00:03:00
Turbine noise measurement	0	Operating	00:10:00
Transition	Toggling 0 -> +20	Operating	00:03:00
Turbine noise measurement	20	Operating	00:40:00
Background noise measurement	20	Stopped	00:10:00
Transition	Toggling +20 -> 0	Starting	00:03:00
Turbine noise measurement	0	Operating	00:10:00
Transition	Toggling 0 -> -10	Operating	00:03:00
Turbine noise measurement	-10	Operating	00:40:00
Background noise measurement	-10	Stopped	00:10:00
Transition	Toggling -10 -> 0	Starting	00:03:00
Turbine noise measurement	0	Operating	00:10:00
Transition	Toggling 0 -> +10	Operating	00:03:00
Turbine noise measurement	10	Operating	00:40:00
Background noise measurement	10	Stopped	00:10:00
Transition	Toggling +10 -> 0	Starting	00:03:00
Turbine noise measurement	0	Operating	00:10:00
Transition	Toggling 0 -> -20	Operating	00:03:00

strong and highly turbulent winds risking to endanger the turbine during yaw misalignment conditions in the late afternoon of the 28th. These above-rated conditions being of less importance to WFFC applications, these data would not have brought much additional value. In total, a little more than 21 hours of measurements were recorded over the four days (4.58 h on day 1, 2.35 h on day 2, 6.13 h on day 3 and 8.07 h on day 4).

The wind conditions observed during the campaign are represented on Fig. 4. Very different conditions were experienced each day : from low to medium wind speeds during the first two days to higher wind speeds on the two last ones. The IEC standard requires a minimum number of 10 samples in each bin. As can be seen on Fig. 5, representing the raw capture matrix derived from the SCADA data recorded during the 6 rounds of the test, this criteria is fulfilled for a large number of wind speeds bins and all yaw positions thanks to those very favorable wind conditions. Consequently, the minimum wind speed range recommended by the standard, 8 to 13.5 m/s (corresponding to 0.8 to 1.3 times the wind speed at 85 % of the turbine rated power), was extended to 6 - 13.5 m/s when analyzing the results.

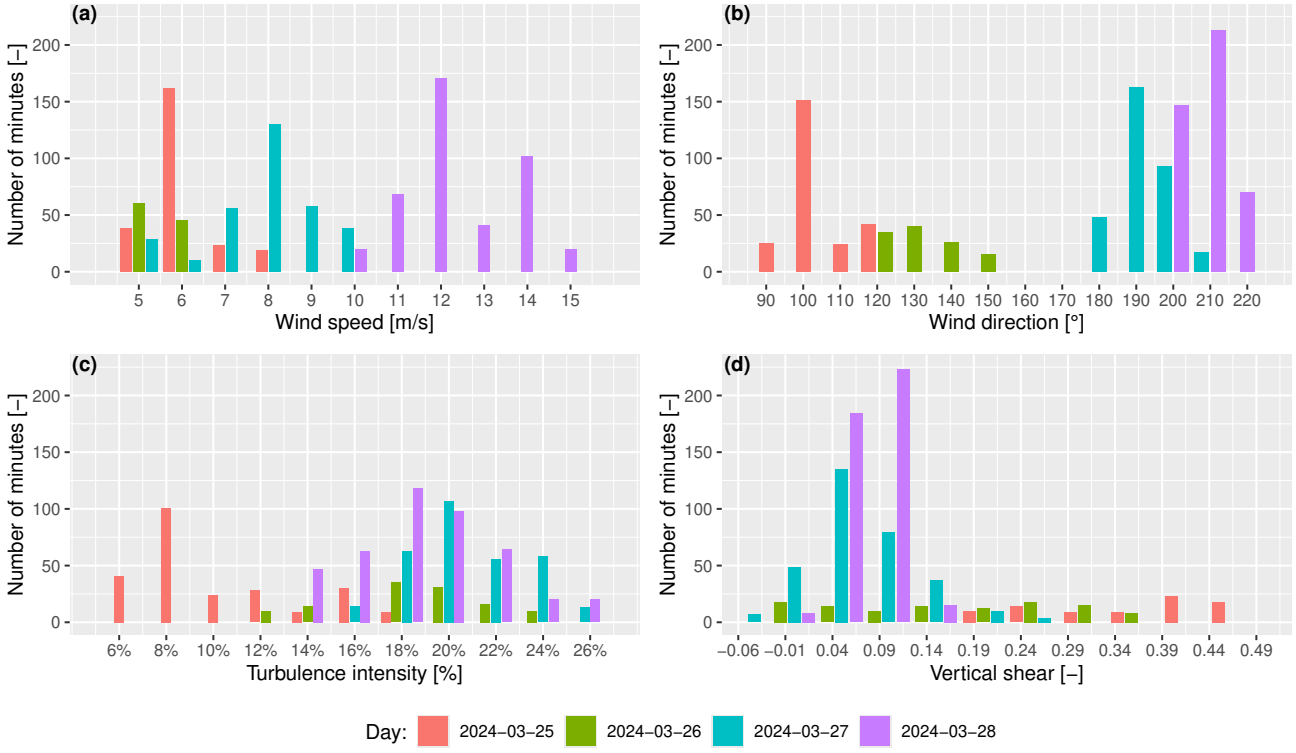

Figure 4. Wind conditions recorded during the field campaign. Histogram of occurrences of wind speed (a), wind direction (b), turbulence intensity (c) and wind shear (d) for each day of measurement.

The wind direction varied from East the first day to South-West the last day, meaning that the turbine was never affected by any wakes during the measurement. Turbulence and shear conditions were estimated using the ground-based Windcube lidar: the lidar measurement at hub height is considered for the turbulence while the wind shear is estimated by fitting a power law to 14 planes of measurement ranging from 40 to 140 m (i.e. the span of the turbine rotor). Both were also very variable depending on the day, with a high shear and a low turbulence observed at the beginning of the week and on the contrary a highly turbulent and low sheared flow noticed at the end of the test.

2.4 Data availability

~~One of the biggest challenge of~~ A significant challenge for a field campaign implicating as many sensors as this one is to maintain the availability of all of them during the periods of measurement. As can be seen on Fig. 6 and Fig. 7, representing the availability of wind related and acoustic sensors, respectively, this challenge was practically met.

Most of the SLMs were also fully available during the test. Unfortunately ~~some sensor defaults introduced a loss on data in some conditions~~a few sensor defaults were observed when preprocessing the data. SLM #04 shows only a 10 % availability

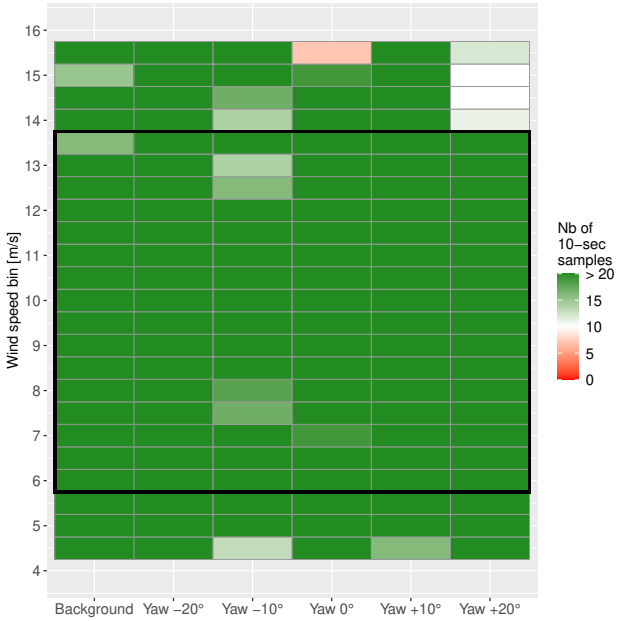

Figure 5. Raw capture matrix for the TWAIN acoustic campaign. The number of ~~10-seconds sample~~ 10-second samples is shown for each wind speed bin and each yaw misalignment case. The black rectangle represents the wind speed range of interest between 6 and 13.5 m/s.

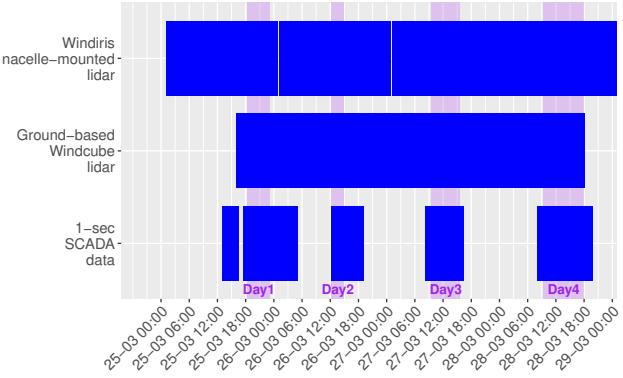

Figure 6. Availability of related wind sensors during the TWAIN acoustic campaign. The shaded purple vertical bands indicate active measurement for each day.

because it was only possible to record data every 10 seconds instead of 1 second due to a logger issue. SLM #07 reports a reduced availability since it was not installed during the second day of measurement. The IEC standard also requires an analysis of 1/3-octave bands between 20 Hz and 10 kHz. A full dataset was obtained for 18 SLMs but 1/3-octave information was missing for SLMs #09 and #18, and incomplete for #04, #10, #16, #21 and #22.

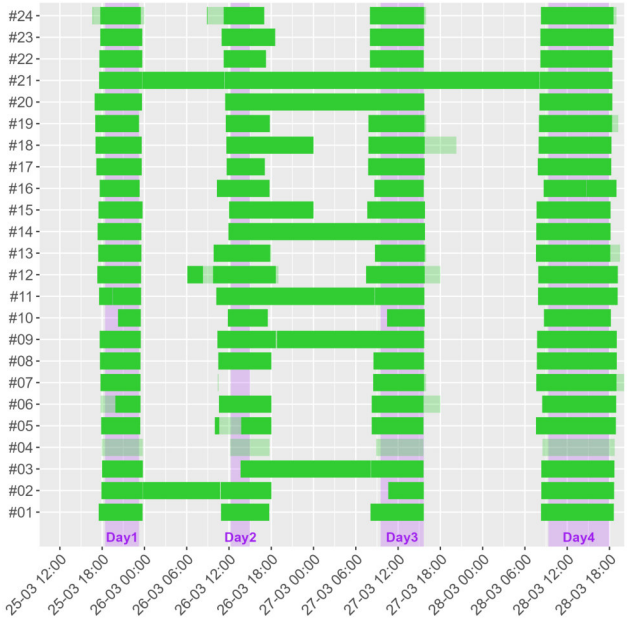

Figure 7. Availability of overall sound pressure level data for all SLMs during the TWAIN acoustic campaign. A transparent band (e.g. for SLM #04) corresponds to a reduced availability. The shaded purple vertical bands indicate active measurement for each day.

Despite these ~~few~~ small inconveniences, the quantity of data collected during the 4 days and 6 rounds of measurement can be considered as satisfactory and ready to be processed for the derivation of the apparent sound power level, as is described in the next section.

3 Data processing

The IEC 61400-11-1standard defines a procedure for the processing of data recorded during an acoustic noise measurement campaign: aggregation of data into 10-secondschunks, time synchronization between acoustics and wind related sensors, estimation of ambient wind speed, normalization of 1/3-octave band spectra and correction for secondary wind screen, sorting into bins, computation of average and standard deviation acoustic values on bin centres and computation of apparent sound power spectra through the difference between the total noise and background noise values.

However, this procedure corresponds to the case of a single SLM placed directly downstream of a turbine aligned with the wind direction. Due to the novelty of this campaign, implicating a large number of SLMs and the application of a yaw misalignment to the turbine, some adjustments to the standard procedure were necessary.

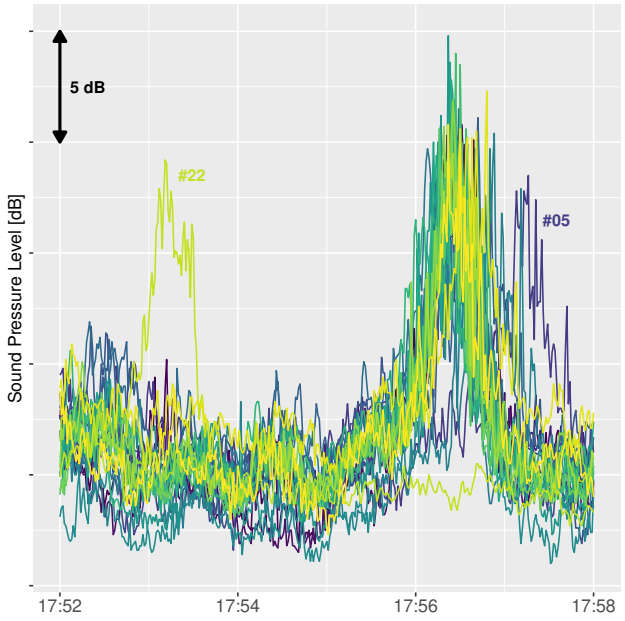

Figure 8. Illustration of a time sync issue during day 4. The passing of plane increases the sound pressure level of all SLMs between 17:56 and 17:57. This is captured by all of them at more or less the same time, except for SLM #22 which seems in advance and SLM #05 which is delayed.

3.1 Acoustic data cleaning

The process described above must be performed on a cleaned dataset. Despite the effort made every day during the campaign to calibrate and check the time synchronization of each SLM before launching a new round of measurement, a few issues were noticed when analyzing the raw acoustics data. Considering the large quantity of data to handle (more than 507 hours when accounting for the 24 ~~microphones~~SLMs), specific post-processing techniques were designed to automatically filter and correct the dataset.

3.1.1 Time synchronization

The ~~biggest issue observed when looking at the data~~ most significant issue observed during data inspection was related to the time synchronization of the acoustic signals. Indeed, during the campaign each SLM was recording data using its own internal clock. Although each clock was verified at the beginning of a new measurement, it proved not enough to ensure a proper synchronization of the signals and time shifts were found when inspecting the recorded time series. These time shifts were seen to be dependent on both the day and the sensor. Figure 8 shows an example in which two ~~microphones~~ SLMs clearly seem out of sync with respect to the rest of the fleet.

In order to massively identify and correct those time shifts, the following methodology was applied for each day of measurement.

1. For each pair of SLMs, a cross-correlation curve is obtained by sliding the time signals by step of 1 second over ± 600 seconds.
2. The time delay that corresponds to the maximum of this cross-correlation curve is inserted into a matrix of time shifts that stores the most likely delay for each couple of SLMs for a given day of measurement.
3. A unique time shift per SLM is deduced by solving a linear optimization problem.
4. Finally, the acoustic signals are resynchronized with the turbine SCADA clock by using another cross correlation analysis with the electrical power signal (and taking advantage of the background noise measurement periods when the power suddenly drops to 0 kW with a an immediate reduction of its noise emissions).

The ~~last step~~ first three steps of the methodology are performed to ensure a better robustness of the clock drift correction thanks to the comparison of multiple SLM pairs. The last one is allowed by the fact that the subject of the study is focused on energetical aspects rather than on acoustic propagation time. The distance between the main acoustic sources (the blade outer part for aerodynamic noise and the nacelle for mechanical noise) is at most around 300 m, so the dispersion of acoustic propagation times remains on the order of a second. Given that the data is then aggregated into ~~10-seconds chunk~~ 10-second chunks for the rest of the IEC analysis, the uncertainty related to this correction ~~can be considered negligible~~ is small. A sensitivity analysis was run on the results by shifting all the acoustics signals by ±1 second, and showed that this effect only had a negligible impact.

A summary of calculated time shift for all SLMs and all day of measurement is proposed on Fig. 9. It can be seen that the vast majority of the introduced corrections are within ± 15 seconds. Nonetheless, significant delays were applied for some SLMs: -547 seconds were found for SLM #15 on days 1 and 2, and +192 seconds were obtained for SLM #22 on day 4 in accordance with the visual observations of Fig. 8.

3.1.2 Noisy events and outliers removal

The requirements of the IEC 61400-11-1 standard indicate that periods with intermittent background noise shall be omitted from the analysis. As already explained in Sect. 2 above, an operator was always present onsite during the period of measurement to take note of the time when noisy events were heard (aircrafts, cars, agricultural machineries, ...). The ~~exact~~ 1-second acoustic signals of each SLMs were visually inspected to identify the starting and ending times of ~~the events were readjusted after a visual inspection of the acoustic signals~~ each event with some security margin (see e.g. Fig. 8 for an example of plane passing) and the corresponding periods were filtered accordingly.

However, despite this first filter based on the observer's notes, it was observed ~~during the visual examination~~ that a few remaining abnormal data could not be related to any recorded noisy events. Those ~~random~~ outliers are characterized by sudden peaks in the acoustic signals. All impulsive events (the external ones as well as the ones originating from the turbine) are

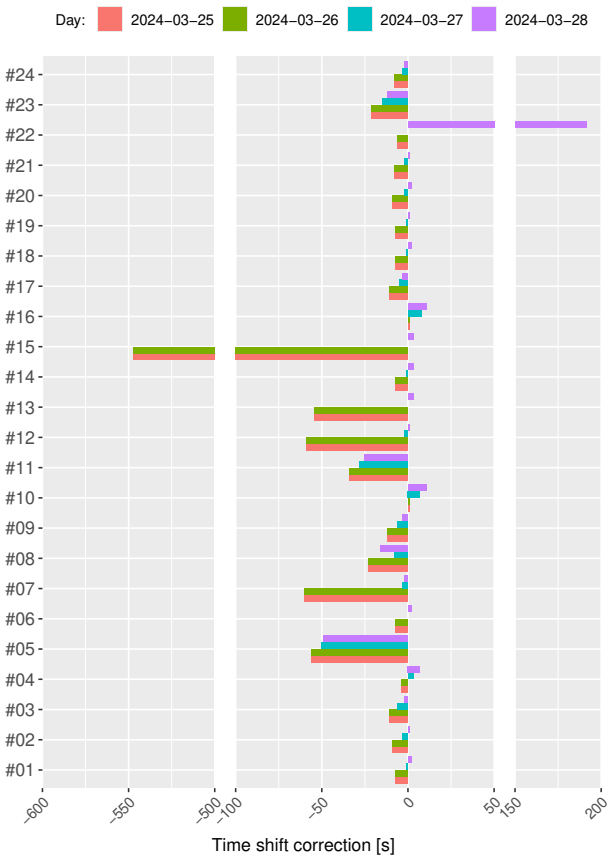

Figure 9. Time shift corrections applied for each ~~microphone~~ SLM and each day of measurement. 0 seconds represents a perfect synchronization with the SCADA, a positive (resp. negative) value is found when the ~~microphone~~ SLM data is ahead (resp. delayed) with respect to the SCADA.

unwanted, as this study primarily is focusing on turbine pseudo-stationnary noise sources. To automatically detect and remove those points, a running median filter (Tukey, 1977) has been set up. Without visual field information, the parameters of the filter have been tuned to automatically reproduce the *a posteriori* detection performed by a human expert on a reduced dataset. The expert was asked to identify obvious outliers in the OASPL time series recorded by SLM #01. The main parameters of the automatic detection tool are the length of the rolling median window, the detection threshold, and the length of the removal window. They have been manually chosen to provide a satisfactory proportion of correctly detected outliers while avoiding false positives. The selected parameter values achieve a recall of 64% (i.e., 64% of expert-identified events are correctly detected) and a precision of 100% with respect to the expert reference, meaning that all automatically detected events correspond to events identified by the expert. In the end, the filter, applied on the full dataset, consists in the following steps: a $\pm$ 50 seconds running median of the acoustic signal is calculated. Every time the original signal goes 10 dB above the running median, an

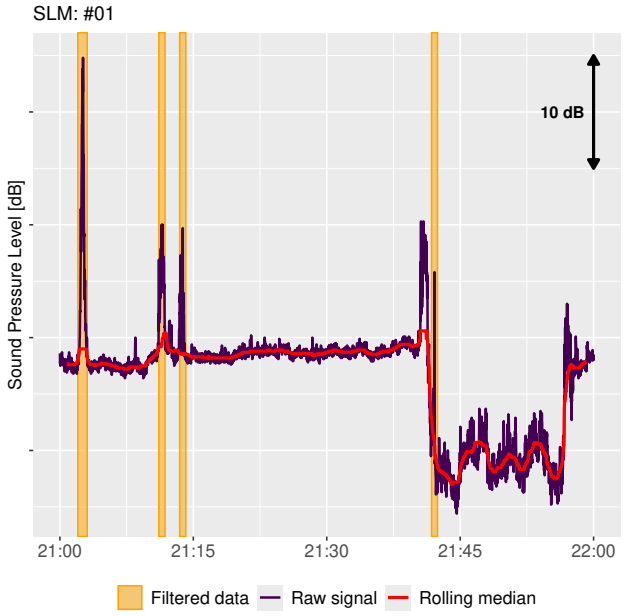

Figure 10. An example of automatic outlier detection for SLM #01. The rolling median is calculated from the raw signal and periods of ± 20 seconds above the + 10 dB threshold are detected and removed. The turbine is shutdown between 21:44 and 21:57.

outlier is marked and data within ± 20 seconds around this point is filtered. The full process is illustrated on Fig. 10. A ~~total of 1963~~ spike in SPL around 21:42 is not removed as an outlier since the level does not reach the +10 dB threshold over the running median. This event is actually believed to originate from the turbine itself, as it systematically appears a few seconds before each turbine stop, occurring here between 21:40 and 21:55. It may be linked to noisy events in the turbine shutdown procedure. Since this phenomenon occurs systematically during an on/off transition, it is naturally filtered out as a transient period since the turbine is setting up to a new operational state.

A total of 2150 outliers were identified thanks to this method for the 24 SLMs over the 4 days of the campaign, with disparate behaviors depending on the sensors. Since the subsequent processing, based on the IEC 61400-11-1 standard, relies heavily on median computations, it is inherently robust to residual outliers, and reasonably independant on the filter parameters values. Repeating the whole data processing with a more restrictive filter, using a level threshold of 5 dB above a ± 25 seconds rolling median, raised the total outliers count to 4616, and showed a minimal mean absolute deviations in output sound power levels (below 0.04 dB).

3.1.3 Final adjustments and aggregation

In addition to these global cleanings applied to all ~~microphones~~SLMs, a few individual adjustments were also implemented ~~on some SLMs~~ to correct specific issues~~that were detected~~.

– SLM #06 showed a very low noise level for a few hours during day 1 despite a normal calibration procedure. This behavior was not repeated the following days of the campaign and could not be explained by the SLM manufacturer other than by a bad connection. ~~Since variations of its signal were consistent with the ones observed at its neighbors, it was finally decided to correct the measures on day 1 by applying a constant +29.5 dB offset, calculated to fit the mean difference observed with the two closest microphones during the 3 other days of the campaign~~These suspicious data have been discarded.

– SLM #21 only recorded 1/1-octave band instead of 1/3-octave data. The 1/3-octave band was obtained through a linear interpolation of the 1/1-octave band data, with the additional constraint of making sure that the sum of energy of the 3 calculated consecutive 1/3-octave bands was consistent with the measured level for the corresponding 1/1-octave band.

After those final corrections, the data preprocessing steps defined in the IEC procedure were followed. All signals were first aggregated into 10-second~~s~~chunks, then the 1/3-octave data were normalized to the measured overall sound pressure level and the correction for the secondary wind screen applied.

3.2 Identification of reference wind conditions

The data reduction procedure described in the IEC standard stipulates that the data must be binned by wind speed. The reference wind speed to be used for the binning is deduced from the active power signal by inverting the turbine power curve. The (adjusted) nacelle anemometer and external wind sensors are used as alternative source of data when the power curve cannot be used (i.e. nominal power reached or turbine stopped for background measurement).

However this methodology is only valid for a turbine that is aligned with the wind. Indeed, the performance of a steering turbine is reduced and no longer follows the expected power curve. Measurements from nacelle anemometers are also known to be unreliable when yaw misalignment is applied on a turbine (Kanev, 2020; Astolfi et al., 2023). It was thus necessary to adapt the IEC methodology to account for the specificity of this test.

For this field campaign, the reference wind speed signal was calculated ~~as follows~~through the following priority order.

1. When the turbine was operating with no yaw misalignment, and the wind speed was within the allowed range for interpolation prescribed by the standard, the active power signal and the power curve were used. These conditions represents approximately 9% of the total dataset. The power curve considered for the interpolation was calculated thanks to the nacelle lidar data over 4 months of measurements from 7 February to 2 June 2024 and according to the procedure of the IEC ~~standard~~ 61400-12-1 standard (IEC, 2017).

2. When the turbine was operating with no yaw misalignment but the wind speed was outside allowed interpolation range, the nacelle anemometer, adjusted with a factor $\kappa_{nac} = 0.984$, was chosen. Only 6% of the data falls into this category.

3. During background noise measurement or when yaw misalignment was applied to the turbine (i.e. the remaining 85 % of the dataset), the measurement of the nacelle lidar at 300 m upstream (2.7 rotor diameters), adjusted with a factor $\kappa_z = 0.931$, was selected.

This sensor was favored over the ~~ground based~~ ground-based lidar because its wind speed measurements were better correlating with the wind speed derived from the active power signal in step 1 above~~.~~, as is shown in Tab. 2. Given that a transient period of 3 minutes was considered between each yaw categories (see the toggle measurement routine in Tab. 1), there were no direct transitions between the nacelle lidar measurement and the SCADA signals, avoiding thus the risk of introducing artifacts between the different sources.

The high frequency measurement of such a lidar is only realized along line of sights (LOS) of the sensor. Data from the 4 LOS must be averaged over a certain time period and combined together to derive the hub height wind speed estimation (Mazoyer and Boquet, 2016). Unfortunately, it proved that the 10-second~~s~~resolution was too short a period to properly achieve this reconstruction: the resulting wind speed signal was too noisy and did not correlate well with the SCADA data. While complex algorithms exist to assess the incoming wind field from high frequency lidar measurements (Raach et al., 2014; Borraccino et al., 2017; Guillemin et al., 2018), another solution was set up instead, for the sake of simplicity. For each day, a constant advection time was calculated using the mean wind speed observed during the period of record and the distance between the upstream lidar measurement range and the turbine. This advection time was used to shift temporally the lidar data and synchronize them with the rotor plane. Finally, wind speed measurements were averaged for every 10-second~~s~~chunks considering a rolling window of 1 minute.

In order to make sure this methodology provides the highest quality signal for the rest of the study, the correlation of various lidar wind speed measurements are compared with the reference signal deduced from priority 1 above, in yaw-aligned conditions only. Table 2 recaps the calculated correlation coefficients. It is confirmed that the nacelle lidar gives a better correlation than the ground-based sensor since its measurement is made closer to the turbine, but that considering a binning period of 10-second only introduces more noise and degrades the correlation with the reference signal. Conversely, the use of a rolling window with a constant advection time significantly improves the results: the obtained signal shows a correlation coefficient close to the one of the nacelle anemometer, considered as priority 2 in the IEC 61400-11-1 standard.

While wind direction is only considered in the IEC standard as a filtering variable, it is for this campaign a quantity of high interest. The experimental setup being fully symmetric, the relative position of each ~~microphone~~ SLM with respect to the turbine is determined based on the absolute wind direction. Like~~wise~~the nacelle anemometer, the turbine wind vane cannot be trusted under yaw misalignment (Rott et al., 2023). To ensure a consistent measure of wind direction during the full test, one of the ~~external sensors~~ lidars had to be used and their correlations to the turbine data ~~at 0° yaw~~ in yaw-aligned conditions were analyzed. The ~~ground based~~ ground-based lidar proved to have the most consistent measure of wind direction and its ~~signal at turbine hub height~~ 10-minutes signal, averaged over all planes of measurement, was therefore selected.

3.3 Derivation of apparent sound power level

Once noise data have been cleaned, and reference wind conditions identified, both datasets can be combined and sorted into bins for both background and total noise to deduce the apparent sound power of the turbine. ~~The following subsections describes how the IEC standard procedure was adapted to account for the particular setup of this field campaign.~~ The diagram shown in Fig. 11 summarizes the data processing methodology applied in this paper and underlines the differences with the current

Table 2. Correlation of lidar wind speed signals with the reference wind speed signal derived from the active power and inverted power curve of the turbine (priority 1). Correlation with the nacelle anemometer signal (priority 2) is also shown for comparison.

Wind speed signal	Correlation coefficient
Ground-based lidar, binned 1-min	0.79
Ground-based lidar, binned 10-sec	0.73
Ground-based lidar, rolling mean 1-min	0.79
Nacelle-mounted lidar, binned 1-min	0.85
Nacelle-mounted lidar, binned 10-sec	0.80
Nacelle-mounted lidar, rolling window 1-min	0.85
Nacelle-mounted lidar, rolling window 1-min + advection	0.90
Nacelle anemometer (priority 2)	0.92

version of IEC 61400-11-1 standard. For the sake of clarity, ~~Tab. 3 recaps the~~ all variables and symbols used in this section ~~.~~ are listed in Tab. 3.

3.3.1 Identification of background noise

With 24 ~~microphones~~ SLMs comes as many estimation of background noise. Figure 12 displays the evolution of background noise measured by the 24 sensors as a function of wind speed. All of them show a clear increasing trend with more or less the same slope. However at a given wind speed significant differences can be noticed, reaching up to approximately 4 dB when considering the two extreme ~~microphones~~SLMs. These gaps can be explained by the variety of local environment around each sensor. For example, SLMs#~~04 installed closer to the substation than SLM~~ 01 to #~~19 which is located in the middle of the field might not show the same background noise level~~ 12 located on the southern section of the circle (see Fig. 2) ~~.~~ tend to display a higher background noise than the other: this could be related to the presence of highway situated approximately 1 km south to the wind turbine. SLMs #23 and #24 show higher background noise compared to their symmetrical counterparts #13 and #14: this could be explained by their location being closer to the substation. Difference in crops cutting around each ~~microphone~~ SLM might also have some influence, especially at high wind speeds.

Due to ~~the large disparity of background noise observed~~ operational constraints and the necessity to fit all measurements within only 4 days, it was not possible to conduct additional tests to characterize more accurately the background noise variations at the site. Because of the large disparity observed between all SLMs, it was thus not possible to extract a single background noise value valid for all ~~SLMs~~ of them as a function of wind speed. Instead the approach proposed by Hamilton et al. (2021) was followed, with a specific background noise dataset binned by wind speed calculated for each SLM.

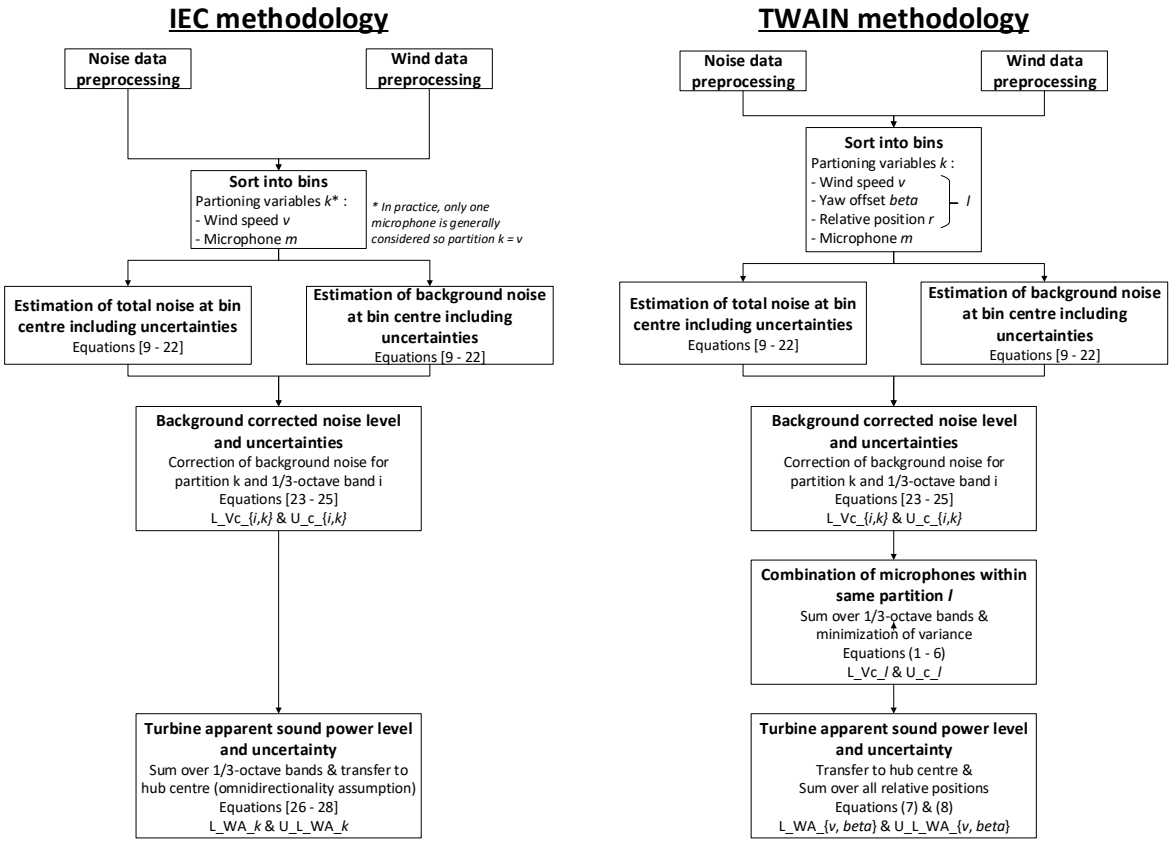

Figure 11. Comparison of data reduction procedure methodology developed in the IEC noise measurement standard (IEC, 2012) (left) and the new methodology proposed for the TWAIN experimental campaign (right). Numbers in brackets [.] refer to equations of the IEC standard, and the ones in parenthesis (.) correspond to equations in this present paper.

3.3.2 Calculation of noise levels

Like~~wise~~the background noise, the total noise dataset is binned by wind speed for each SLM. However compared to the IEC standard two additional variables must be taken into account: one is of course the yaw ~~offset~~ misalignment angle applied to the turbine and the second is the relative position of the SLM with respect to the wind direction. Indeed, the noise pattern emitted by a turbine is not homogeneous and depending on the wind direction, the SLM will not measure the same sound pressure level. For each 10-second~~s~~chunk, the relative position of a SLM was calculated as the difference between the reference wind direction and the azimuth between the turbine and the SLM, and rounded to the closest 15° bin. Consequently it is no longer

Table 3. List of symbols considered in the data reduction procedure. The first section defines the physical variables used as subscripts, the second the data partition used in the procedure, and the third the acoustic-related quantities calculated. The subscript letter c is taken from the IEC ~~61400-11~~ 61400-11-1 standard and refers to the background noise correction.

Symbol	Variable
i	1/3-octave band
v	Wind speed bin
m	Sound Level Meter (SLM)
r	Relative position
β	Yaw ~~offset~~ misalignment category
$k = \{v; \beta; r; m\}$	Partition defining a given wind speed, yaw category, relative position and SLM
N_k	Number of data points in partition k
$l = \{v; \beta; r\}$	Partition defining a given wind speed, yaw category, relative position
N_l	Number of data points in partition l
M_l	Number of SLM m that can be combined together in partition l
w_k	Weight of each ~~microphone~~ SLM within partition l
$L_{Vc_{i,k}}$, $u_{c_{i,k}}$	1/3-octave band background-corrected sound pressure level (SPL) and corresponding uncertainty
L_{Vc_k}, u_{c_k}	Background-corrected SPL and corresponding uncertainty (aggregation over all 1/3-octave bands)
L_{Vc_l}, u_{c_l}	Background-corrected SPL and corresponding uncertainty (aggregation over all ~~microphones~~ SLMs m within partition l)
$L_{WA,\{v,\beta\}}$, $u_{L_{WA,\{v,\beta\}}}$	Turbine apparent sound power level and corresponding uncertainty (combination over all relative positions r)

required to filter data when wind direction is changing by more than 15° as recommended in the IEC standard, the data are simply redispatched between the 24 SLMs of the circle.

Still, the supplementary partitioning added by this new binning variable complexifies the data processing. Due to the curse of dimensionality, with these 4 binning variables some of bins find themselves very sparsely populated. Accounting at this stage for the minimum number of 10 samples in each bin would discard a very large number of them (approximately 45 %). Alternatively, to retain as much data as possible, a much smaller value of 3 samples per bin was used. ~~Then the~~ Note that this reduction is a temporary adjustment. It will compensated for later in the procedure by imposing a minimum of 10 *cumulative* samples across SLMs, for each set point (wind speed bin, relative position, and yaw angle).

The formula of the IEC noise standard were then applied to every bin in order to calculate the average wind speed and sound pressure level in each 1/3-octave bands, evaluate the corresponding uncertainties and covariance, and interpolate the noise levels at bin centre including uncertainties. ~~The Tab.~~ Table 4 summarizes the values that were taken for the type B uncertainties. It must be noted that an additional source of uncertainty can arise from the assessment of the turbine yaw misalignment and the

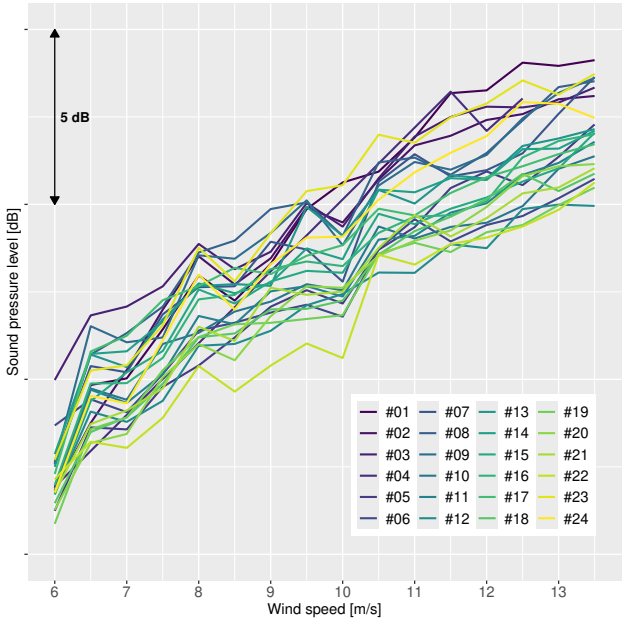

Figure 12. Evolution of median background noise as a function of wind speed bin for each SLM surrounding the wind turbine.

Table 4. Type B measurement uncertainties

Component	Chosen value	Remark
Calibration, u_{B1}	0.2 dB	IEC ~~61400-11~~ 61400-11-1 proposed value
Instrument, u_{B2}	0.2 - 0.8 dB	Frequency dependent, based on a calibration certificate
Board, u_{B3}	0.3 dB	IEC ~~61400-11~~ 61400-11-1 proposed value
Wind screen, u_{B4}	0.2 - 0.9 dB	Frequency dependent, based on a calibration sheet
Distance and direction, u_{B5}	0.1 dB	IEC ~~61400-11~~ 61400-11-1 proposed value
Air absorption, u_{B6}	0 dB	IEC ~~61400-11~~ 61400-11-1 recommendation
Weather conditions, u_{B7}	0.5 dB	IEC ~~61400-11~~ 61400-11-1 proposed value
Wind speed, measured, u_{B8}	0.7 m/s	IEC ~~61400-11~~ 61400-11-1 proposed value
Wind speed, derived, u_{B8}	0.2 m/s	IEC ~~61400-11~~ 61400-11-1 proposed value
Wind speed, power curve, u_{B9}	0.2 m/s	IEC ~~61400-11~~ 61400-11-1 proposed value

slow reaction of its controller to wind direction changes (McKay et al., 2014). However, this error is not listed in the IEC noise standard, and therefore not considered in this paper.

Next, the binned total noise noise is compared to the binned background noise for each ~~microphone~~SLM. Again, the process indicated by the standard was followed to obtain the background corrected sound pressure level at bin centre for each 1/3-octave

band i within each partition of wind speed v, SLM m, relative position r and yaw ~~offset~~ misalignment angle β. The number of samples N_k associated to each partition k (where $k = \{v; \beta; r; m\}$) is taken as the lowest number of samples between the total noise and background noise datasets.

The end of the data reduction procedure differs from the one developed in the standard. Rather than calculating the sound power level for each 1/3-octave band, the background corrected overall A-weighted sound pressure level (OASPL) L_{Vc_k} is calculated for each k by energy summing of all 1/3-octave band background corrected sound pressure values $L_{Vc_{i,k}}$.

$$L_{Vc_k} = 10 \cdot \log\left(\sum_{i=1}^{28} 10^{\left(\frac{L_{Vc_{i,k}}}{10}\right)}\right) \tag{1}$$

For SLM with missing 1/3-octave bands, the measured OASPL was directly used. For those with incomplete 1/3-octave bands, the energy summation is done on the available bands, given that they were previously normalized to match the measured overall sound pressure level. The uncertainty u_{c_k} associated to the obtained OASPL is deduced from the uncertainty of each 1/3-octave pressure value $u_{c_{i,k}}$:

$$u_{c_k} = \frac{\sum_{i=1}^{28} u_{c_{i,k}} 10^{\left(\frac{L_{Vc_{i,k}}}{10}\right)}}{\sum_{i=1}^{28} 10^{\left(\frac{L_{Vc_{i,k}}}{10}\right)}} \tag{2}$$

Finally, the OASPL calculated for several ~~microphones~~ SLMs for the same wind speed, relative position and yaw category are combined into a single value. This is done by computing a weighted average of L_{Vc_k} values over all ~~microphones~~ SLMs within the same partition $l = \{v; \beta; r\}$:

$$L_{Vc_l} = 10 \cdot \log\left(\frac{\sum_{m=1}^{M_l} w_k 10^{\left(\frac{L_{Vc_k}}{10}\right)}}{\sum_{m=1}^{M_l} w_k}\right) \tag{3}$$

with the corresponding uncertainty

$$u_{c_l} = \sqrt{\frac{1}{\sum_{m=1}^{M_l} w_k}} \tag{4}$$

where M_l is total number of ~~microphones~~ SLMs in the partition l, and the weights w_k are chosen to minimize the variance of the derived estimator (Shahar, 2017):

$$w_k = \frac{1}{u_{c_k}^2} \tag{5}$$

The total number of samples associated to the partition l is simply the sum of samples for all partitions k :

$$N_l = \sum_{m=1}^{M_l} N_k \tag{6}$$

Only the partitions with $N_l \geq 10$ are kept for the end of the analysis. Thus, it fulfills the IEC constraint that at least 10 samples must be present in each bin, only that it is allowed that samples can come from multiple sensors to keep as much data as

possible. With the applied process, ~~microphones~~ SLMs with the lowest uncertainty u_{c_k} (generally because they have more samples in their partition) will have a stronger weight w_k and will contribute more to the derived OASPL value.

~~The diagram shown in Fig. 11 recaps the data processing and underlines the differences with the current version of IEC 61400-11 standard.~~

~~Comparison of data reduction procedure methodology developed in the IEC noise measurement standard (IEC, 2012) (left) and the new methodology proposed for the TWAIN experimental campaign (right). Numbers in brackets .refer to equations of the IEC standard, and the ones in parenthesis (.) correspond to equations in this present paper.~~

3.3.3 Aggregation from noise levels to turbine apparent sound power level

Once the sound pressure values have been obtained for each relative position, they can be aggregated together to derive the turbine apparent overall A-weighted sound power level (OASWL) for each wind speed and yaw position $L_{WA,\{v,\beta\}}$. While *sound pressure level* (SPL) is a local quantity, quantifiying the noise level at a specific point in space possibly arising from many noise sources, *sound power level* (SWL) quantifies the acoustic energy flux radiated in the atmosphere in all directions from a specific source. Sound power is fundamentally linked to the surface integration of the squared sound pressure field around a source of interest. The term *overall* is related to the integration of all acoustic frequency components, typically between 20 Hz and 20 kHz.

Contrary to the IEC standard that considers a single ~~microphone~~ SLM located downstream with an omnidirectionality assumption for the noise emission, this novel experimental setup allows for more finesse by accounting for the azimuthal dependence in the estimation of acoustic power. The single contributions at each relative position around the turbine are energy summed, with the hypothesis that the acoustic level is constant over a slice of the hemisphere with an area $4\pi R_1^2\tau$, where R_1 = 161.1 m is the average distance between all ~~microphones~~ SLMs and the rotor centre, and τ = 1/24 is the angular slice ratio associated to each relative position r. This yields the following equations for $L_{WA,\{v,\beta\}}$ and its respective uncertainty $u_{L_{WA,\{v,\beta\}}}$ (Finez et al., 2025):

$$L_{WA,\{v,\beta\}} = 10 \cdot \log\left(\sum_{r=1}^{24} 10^{\left(\frac{L_{Vc_l}-6}{10}\right)} \frac{4\pi R_1^2}{S_0}\tau\right) \tag{7}$$

$$u_{L_{WA,\{v,\beta\}}} = \frac{\sum_{r=1}^{24} u_{c,l} 10^{\left(\frac{L_{Vc_l}-6}{10}\right)} \frac{4\pi R_1^2}{S_0}\tau}{\sum_{r=1}^{24} 10^{\left(\frac{L_{Vc_l}-6}{10}\right)} \frac{4\pi R_1^2}{S_0}\tau} \tag{8}$$

where S_0 = 1 m^2 is a reference area. A linear interpolation from adjacent observer positions r is operated in case of missing L_{Vc_l} values due to a lack of measurement data. If more than 4 points out of the 24 positions were missing for a given wind speed and yaw ~~offset case~~misalignment category, the corresponding OASWL value was not calculated.

With Eq. 7, the effect of yaw misalignment on turbine apparent sound power can be properly estimated, without being biased by the rotation of the noise directivity pattern, as will be discussed in the next section.

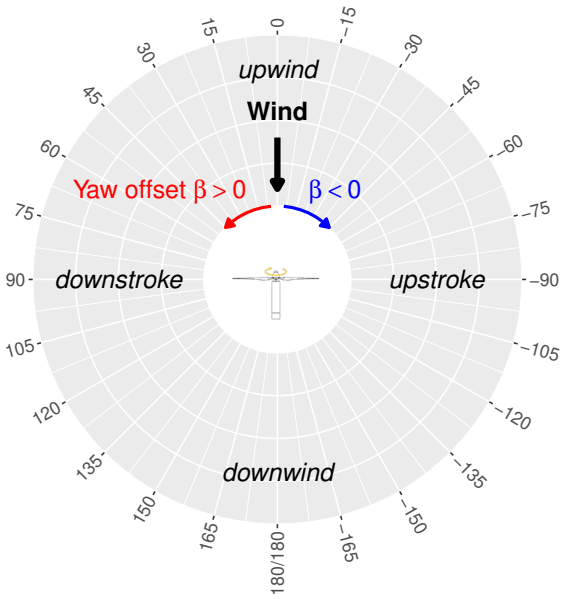

Figure 13. Sign convention followed for the display of the directivity patterns as a function of the observer angle θ. Wind direction is always coming from the angle θ = 0°, while θ = -180°/180° is the downwind position. Positive yaw angles β are defined as a counter-clockwise rotation of the nacelle when seen from above. Positive and negative relative positions corresponds to the downstroke and upstroke side of the rotor plane, respectively.

4 Results and discussion

Following the data processing methodology described in Sect. 3, noise directivity patterns are calculated on the measurement data and presented in this section. In order to harmonize the results coming from multiple wind directions, the sign conventions defined on Fig. 13 are adopted. First, turbine noise emissions are analyzed when it is aligned with the wind in Sect. 4.1, then the effect yaw misalignment is compared to the ~~no yaw~~ yaw-aligned situation in Sect. 4.2.

4.1 Directivity of turbine noise emissions with no misalignment

OASPL of the estimated turbine noise are presented in Fig. 14 for each observer position relative to the nacelle axis without yaw misalignment and across four wind speed bins. Since the turbine reaches rated power at 12 m/s, the selected wind speeds correspond to 52% to 100% of rated power. At all observed wind speeds, OASPL variations in the ground-based directivity pattern reach up to 4 dB(A). In each plot, a region of low noise levels is observed near the rotor plane, sometimes referred to as "noise dips" in the literature (Oerlemans and Schepers, 2009). Within these dips, sound levels are consistently 3.5 to 4.0 dB(A) lower than the maximum values in the corresponding directivity pattern. At lower speeds (7.5 and 9.5 m/s), the minimum

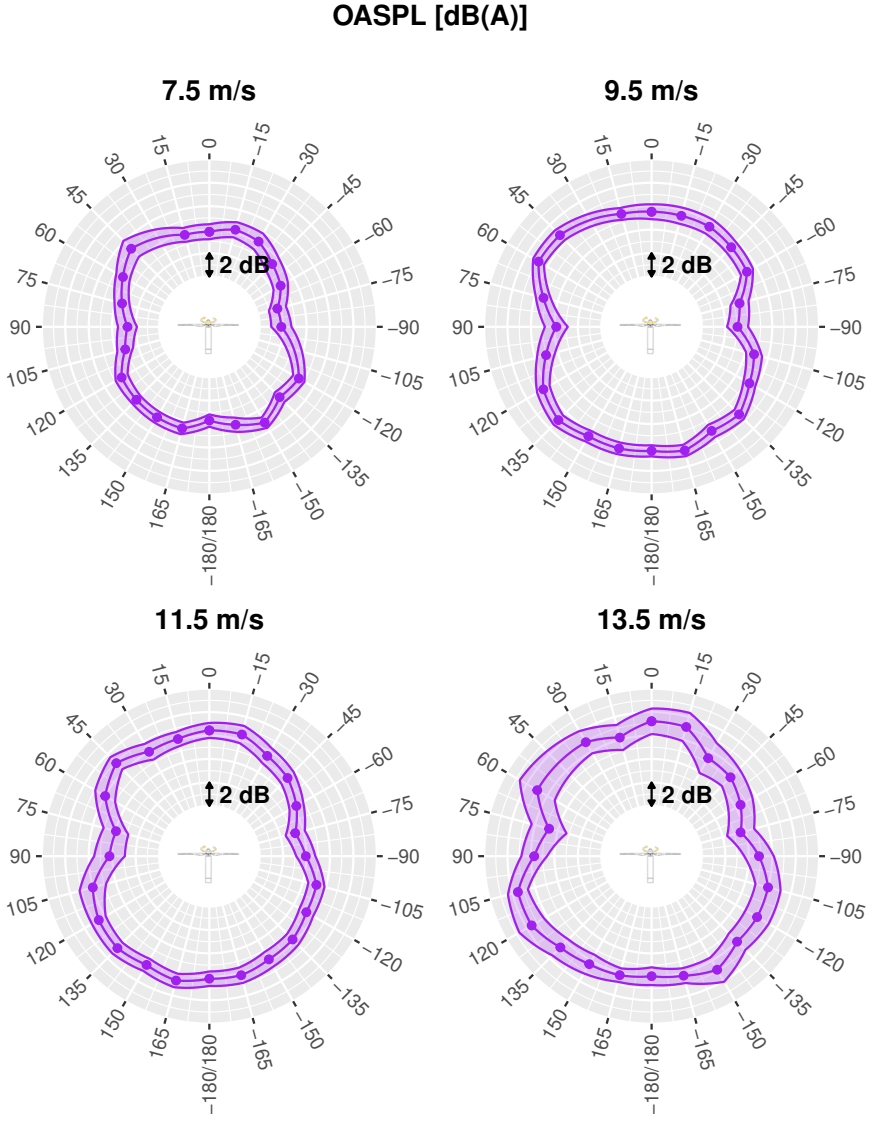

Figure 14. Directivity of overall A-weighted sound pressure level (OASPL) for 4 different wind speeds. In each graph, the wind is coming from the top (position 0°), positive and negatives angles corresponds to downstroke and upstroke side of the rotor, respectively. The shaded ribbon represents one standard uncertainty associated to each OASPL value u_{c_l}, while the point markers indicate the mean value L_{Vc_l}. For observer positions containing less than 10 valid samples, the corresponding data point is omitted.

noise levels occur at observer angles of $\theta = \pm 90°$. Interestingly near rated power (11.5 m/s and 13.5 m/s), the noise dips shift upstream, appearing at $\theta = \pm 75°$.

The direction of the maximum noise level is not aligned with the downstream flow axis, but rather occurs at off-axis positions, either upstream or downstream of the turbine. Specifically, the peak noise levels are observed at $\theta = -150°$ at 7.5 m/s, $\theta = 135°$

at 9.5 m/s, $\theta = 45°$ at 11.5 m/s and $\theta = 120°$ at 13.5 m/s. These levels exceed the axial downstream measurement by 1.4, 0.7, 0.8 and 1.6 dB(A) respectively. This observation is not captured by most existing analytical and semi-empirical models (Bertagnolio et al., 2023) which typically predict symmetric directivity patterns with the maximum aligned along the main flow axis. In contrast, the directivity patterns shown in Fig. 14 exhibit slight asymmetries, not only with respect to the nacelle axis, but also relative to the rotor plane. Since the observed differences in noise levels remain within the uncertainty bounds, a statistical paired t-test was conducted to support this visual observation. The test is based on the level difference between two symmetrical positions $\Delta L_{V,\theta} = L_{V,\theta} - L_{V,\theta'}$ for the same wind speed bin, where θ' is chosen as:

- $\theta' = -\theta$ to test the down-upstroke symmetry and
- $\theta' = 90° - \theta$ to test the down-upwind symmetry.

The set of available observation angle pairs $(\theta; \theta')$ is noted Θ and consists of 207 observations in both of the above mentioned cases. The level difference $\Delta L_{V,\theta}$ is associated with a combined variance u_θ^2 such as

$$u_\theta^2 = u_{c,\theta}^2 + u_{c,\theta'}^2 - 2\rho\, u_{c,\theta}\, u_{c,\theta'} \tag{9}$$

where ρ is the correlation factor between the θ and θ' series, which may be non-zero due to the previously identified noise dips. Following the approach in Eqs. 3 - 5, the weights are defined as the inverse of the combined variance $w_\theta = 1/u_\theta^2$ and the weighted average of the level difference is computed as:

$$\overline{\Delta L}_V = \frac{\sum_{\theta\in\Theta} w_\theta \Delta L_{V,\theta}}{\sum_{\theta\in\Theta} w_\theta} \tag{10}$$

with the standard error

$$\sigma_{\Delta L} = \sqrt{\frac{1}{\sum_{\theta\in\Theta} w_\theta}}. \tag{11}$$

This enables to use the test statistics $t = \overline{\Delta L}_V / \sigma_{\Delta L}$ which is applied across the full set of available wind speed bins at once, using a significance level of 5% and assuming a normal distribution. On average, the OASPL value on the downstroke side is found to be 0.6 dB higher than on the upstroke side. The 95 % confidence interval is [0.5 ; 0.8] dB, associated to a p-value $p < 10^{-6}$, indicating a highly significant left/right asymmetry in the directivity pattern. This result was found to be virtually independant of the correlation factor ρ within the range 0 to 0.5.

The same approach was applied to assess the symmetry between downwind and upwind directions. On average, the sound level measured on the downwind side was 0.4 dB higher than that on the upwind side, at observer positions symmetric with respect to the rotor plane. The 95% confidence interval for this difference is [0.3; 0.6] dB(A), associated to a p-value $p < 10^{-8}$, indicating again a highly significant asymmetry.

From this analysis, it can be concluded that the directivity footprint of the turbine exhibits, on average, higher noise levels on the downstroke side compared to the upstroke side by 0.6 dB(A), and higher levels on the downwind side compared to the upwind side by 0.4 dB(A). These slight asymmetries in the turbine's noise radiation may result from the intrinsic directivity

of elementary acoustic sources. Analytical models based on flat plate assumptions (as for instance Tian and Cotté (2016)) as well as (semi-)empirical models derived from symmetric airfoil measurements (Bertagnolio et al., 2023) do not reproduce such asymmetries. However, camber has been shown to cause deviations of up to 1 dB(A) between the pressure and the suction side noise radiation of an non symmetrical airfoil (Roger and Moreau, 2010). This behavior has also been captured in high-fidelity numerical simulations of cambered and loaded airfoils equipped with serrations (Romani et al., 2021). Thus, the turbine blade camber may be responsible for an asymmetric radiation on both side of the airfoils. As the chordline is more or less contained in the rotation plane, it may result in a upstream/downstream asymmetry in noise levels at the turbine level. The left/right asymmetry is more likely to be linked to both the trailing edge noise directivity and the acoustic amplification term as already proposed by Oerlemans et al. (2007).

Spectral directivity patterns at near-rated power (11.5 m/s) are presented in Fig. 15 over a selected frequency range. At very low frequencies (e.g., 50 Hz), the pattern exhibits two distinct lobes oriented upstream and downstream, with higher levels on the downstream side. Pronounced noise dips are also observed, with sound levels up to 6 dB lower than at the axial downwind position, which corresponds to the direction of maximum noise emission at this frequency. As frequency increases, the directivity pattern becomes more complex, featuring several off-axis lobes. For instance, in the mid-frequency range around 1000 Hz—where human hearing is most sensitive—a narrow lobe centered at $\theta = 45°$ emerges, with noise levels approximately 4 dB higher than adjacent directions. A secondary, less pronounced lobe appears on the descending blade side around $\theta = 120°$. These features are also reflected in the OASPL directivity patterns (lower left part of Fig. 14) at $\theta = 45°$ and $\theta = 135°$. At higher frequencies (e.g., 5000 Hz), the pattern displays multiple lobes with significant local variations and increased uncertainty (± 2.0 dB), compared to lower frequencies. This uncertainty increase is due to a higher data dispersion at 5 kHz than at lower frequencies ("type A" component).

A complementary perspective is provided in Fig. 16 which compares frequency spectra at selected observer positions. In Fig. 16 (a) the maxima of the two OASPL lobes at 11.5 m/s – located at $\theta = 45°$ and $\theta = 135°$ are compared to the reference axial downstream position ($\theta = 180°$). At these two positions, the spectral content shows a pronounced mid-frequency component between 800 Hz and 2000 Hz with increases of 5 dB and 3 dB respectively, relative to the reference. The very high frequency range (above 5000 Hz), further increases of +7 dB and +5 dB are observed. Conversely a reduction in the low-frequency range (50 Hz - 500 Hz) is noted, particularly at $\theta = 45°$, where levels are 7 dB(A) lower than the reference.

Figure 16 (b) presents two additional measurement points at the same wind speed, comparing positions in the rotor plane to the axial downwind reference. In the noise dip regions, the low-frequency content is significantly reduced – by up to 10 dB at 100 Hz. In contrast, an increase in the very high-frequency range is observed, especially on the descending blade side ($\theta = 90°$). In summary, at this specific wind speed, the spectral analysis reveals a strong broadband component in the mid-frequency range at off-axis lobes maxima, as well as a spectral shift toward higher frequencies in the noise dip regions, relative to the axial downwind position.

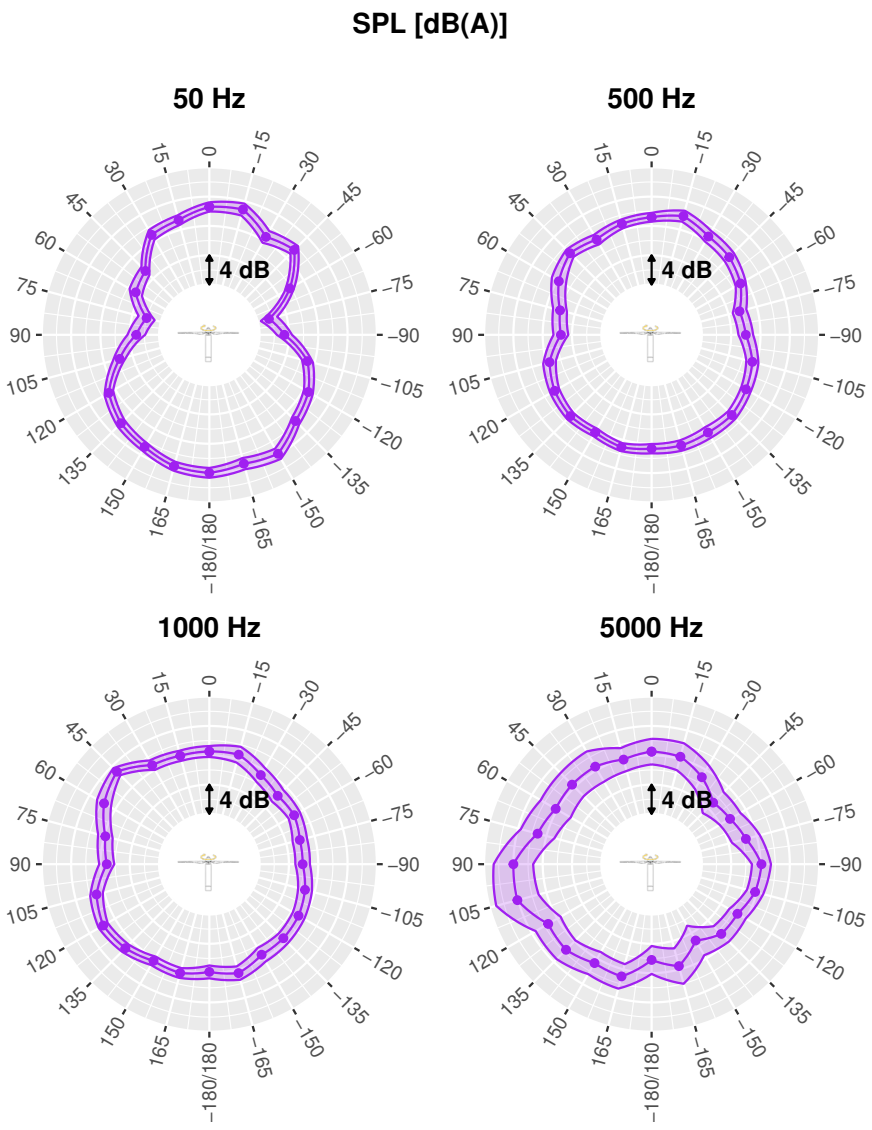

Figure 15. Directivity of ~~overall~~ A-weighted sound pressure level (~~OASPL~~SPL) at 11.5 m/s for 4 different 1/3-octave bands, without yaw misalignement. The shaded ribbon represents one standard uncertainty.

4.2 Effect of yaw misalignment

480 Directivity patterns under intentional yaw misalignment are illustrated in Fig 17 at 9.5 m/s and 11.5 m/s. The first row shows positive yaw ~~offsets~~ misalignment angles (i.e., the ascending blade is oriented toward the incoming flow), while the second row presents negative yaw ~~offsets~~ misalignment angles (i.e., the ascending blade is oriented away from the flow). A first observation is that yaw misalignment does not lead to dramatic changes in overall noise levels. The most prominent effect of

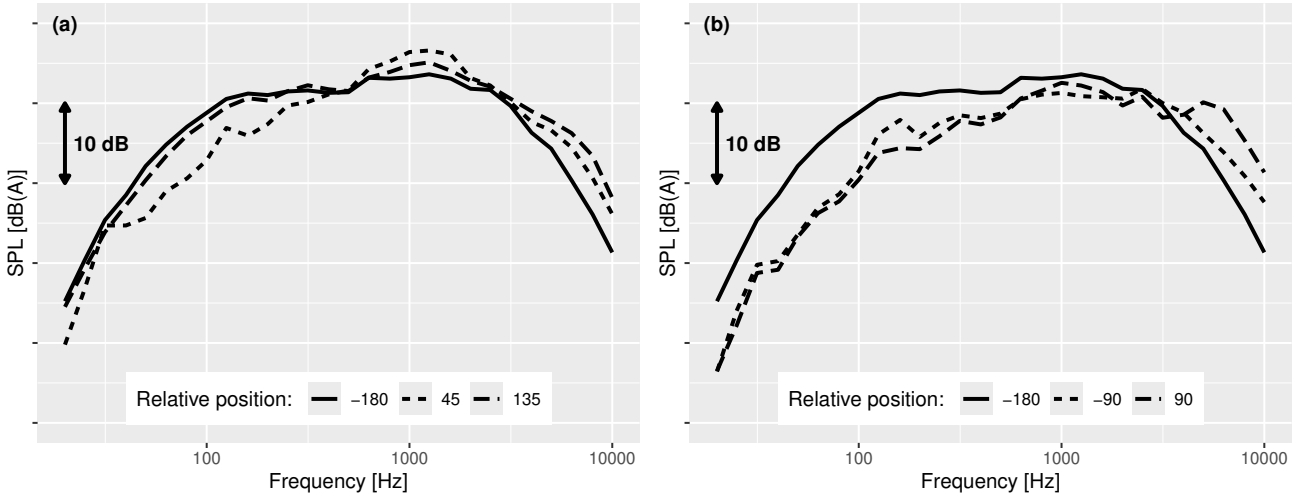

Figure 16. Noise spectra measured at 11.5 m/s. The sound pressure level (SPL) is represented for different positions of the circle. On the left (a), spectra at the two lobes of the directivity pattern (45° for the upstream lobe, 135° for the downstream) are compared to the spectrum at central downstream location (180°). On the right (b), spectra in the rotor plane (90° for upstroke, -90° for downstroke) are compared to the downstream location (180°). Y-axes are consistent between the two sub-figures.

steering the turbine away from the main flow direction is a rotation of the entire directivity pattern, which appears to remain aligned with the turbine orientation in all four cases – particularly around the recognizable noise dip regions. It is worth noting that the yaw angle sampling step $\Delta\beta = 10°$ is not a multiple of the observer angle sampling step $\Delta\theta = 15°$, which explains why the noise dips may appear at similar positions for different yaw angles. Some regions appear more strongly influenced by the flow direction than by the turbine orientation and are amplified when a yaw ~~offset~~ misalignment is applied. This is particularly evident in the upwind-upstroke sector $[0°; -45°]$ for $\beta > 0$ and in the upwind-downstroke sector $[0°; +45°]$ for $\beta < 0$. In general, larger absolute yaw ~~offsets~~ misalignment angles β tend to introduce greater complexity into the directivity pattern.

Spectral variations in the directivity patterns at $v = 11.5$ m/s are illustrated in Fig. 18. At the lowest frequencies (50 Hz), the rotation of the directivity pattern induced by the turbine misalignement is particularly visible. The most significant variations with respect to the yaw misalignment angle β are predominantly localized near the rotor plane ($|\theta| \simeq 90°$). ~~The~~ However, the acoustic impact of yaw ~~offset is more evident at the lower~~ misalignment in the lowest frequency range (50 Hz) ~~and upper (5000 Hz) ends of the frequency spectrum, compared to the mid-range frequencies (500 Hzand 1000 Hz) . This behavior may be attributed to the relative variations of different noise generation mechanisms: turbulent inflow noise , which usually dominates at low frequencies, and~~ cannot be reduced to a rotation. The simple 2-lobes pattern of the aligned case cannot be recognized at other yaw angles, showing a more complex structure. It may be the expression of a significant change in the prominent aeroacoustic sources at this frequency. Interestingly, this is not the case for most of the other plots at higher frequencies in

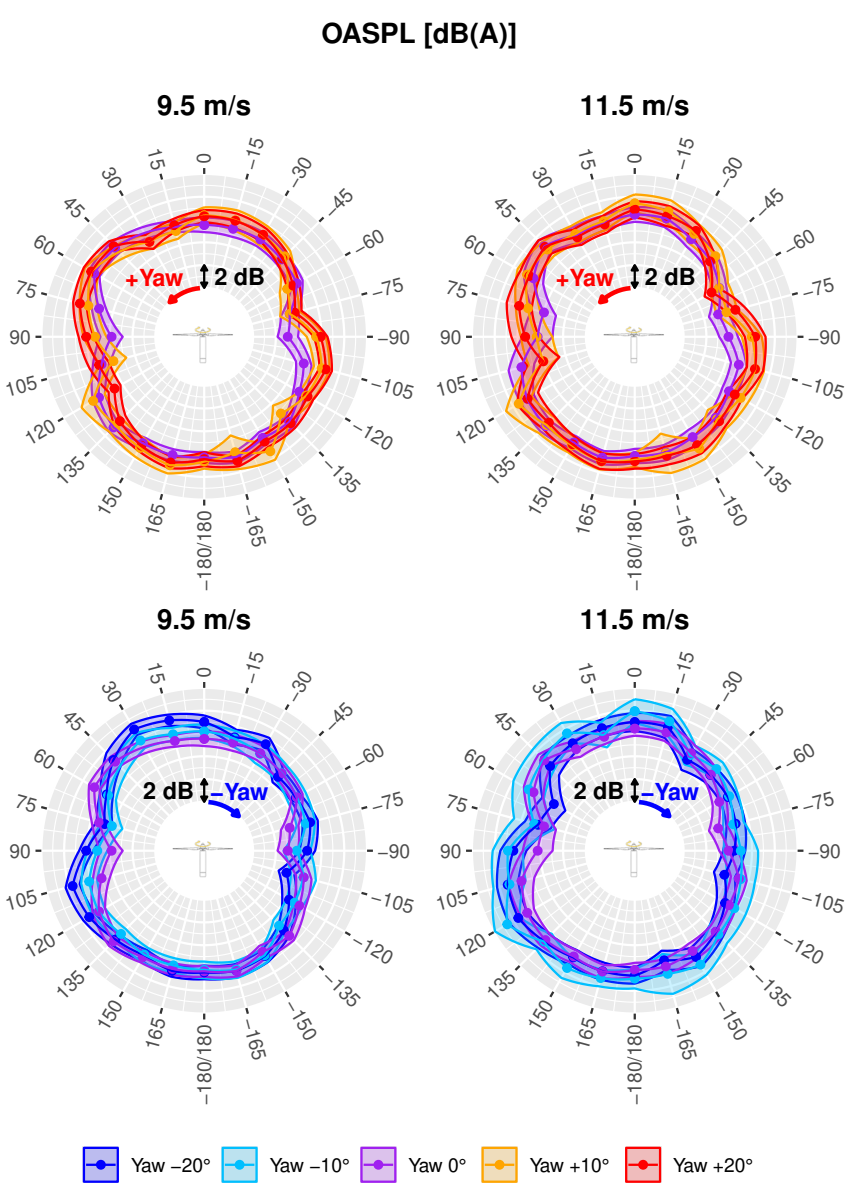

Figure 17. Directivity of overall A-weighted sound pressure level (OASPL) for positive (top) and negative (bottom) yaws, and 2 different wind speeds. In each graph, the wind is coming from the top (position 0°), positive and negatives angles corresponds to downstroke and upstroke side of the rotor, respectively. The shaded ribbon represents one standard uncertainty associated to each OASPL value u_{c_l}, while the point markers indicate the mean value L_{Vc_l}. For observer position containing less than 10 valid samples, the corresponding data point is omitted.

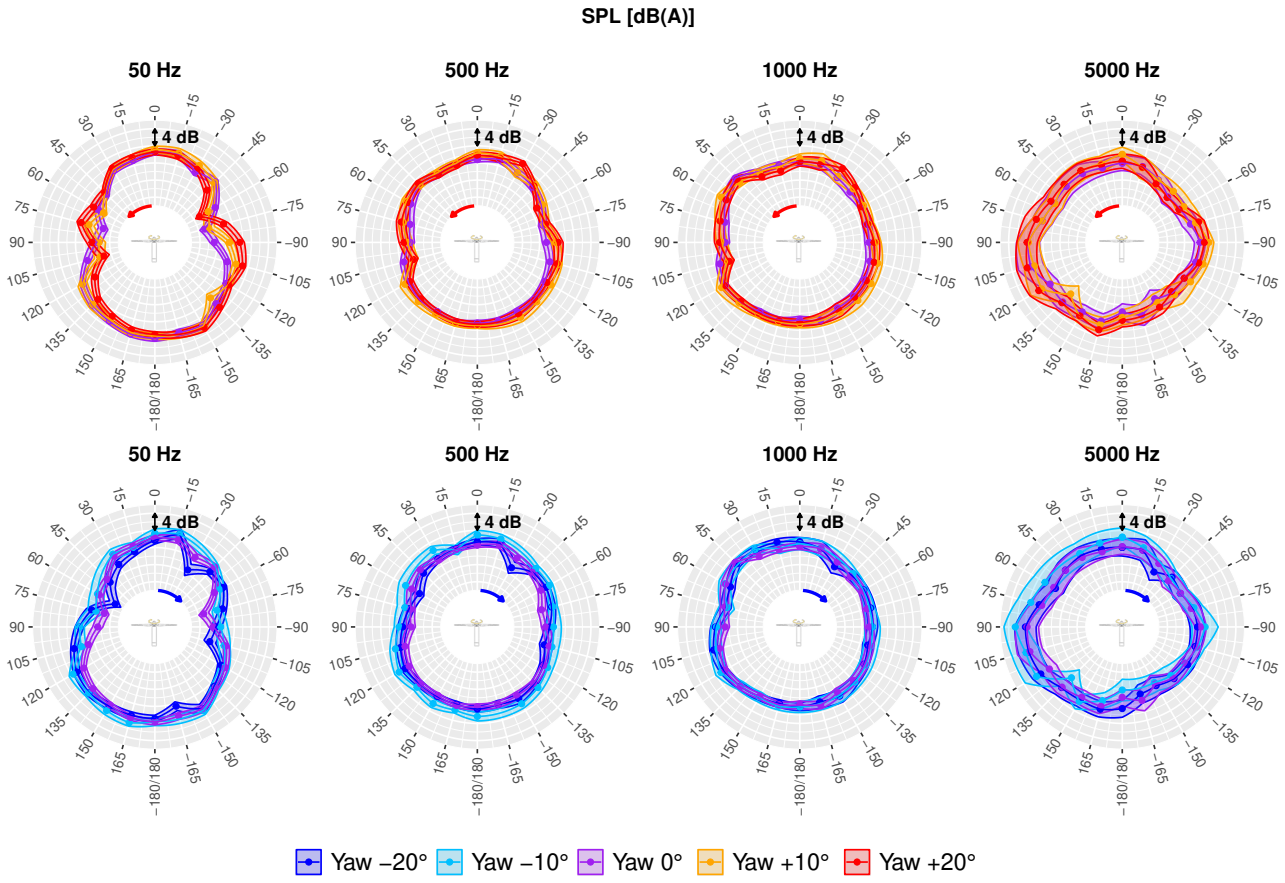

Figure 18. Directivity of A-weighted sound pressure level (SPL) at 11.5 m/s for positive (top) and negative (bottom) ~~yaws~~yaw angles, and 4 different 1/3-octave bands. The shaded ribbon represents one standard uncertainty.

Fig. 18. It is generally accepted that wind turbine aerodynamic noise is dominated by the turbulent boundary layer - trailing edge noise (TBL-TE) in the higher frequency range, typically above 800 Hz, and by the turbulent inflow (TI) noise at lower frequencies. If this holds for the current turbine, it would suggest that the yaw misalignment has a strong on influence on the TI component and virtually not on the TBL-TE component, at least up to 5 kHz. TI noise is produced by the interaction between turbulent eddies in the atmosphere with the moving leading edge of the three blades. In yaw-aligned conditions, a scaling variable of TI noise models is the integral length scale of the atmospheric turbulence. The correlation and phase relationship between the relative normal wind velocity component encountered by different sections of a blade are indeed important, as they can reinforce or mitigate the noise production process. A typical signature of this relationship at the airfoil level is its noise directivity pattern. As the turbine is yawed, the blades passes through atmospheric turbulence with an angle. With the turbulence longitudinal correlation, this angle may increase the apparent length scale and reinforce the TI noise production

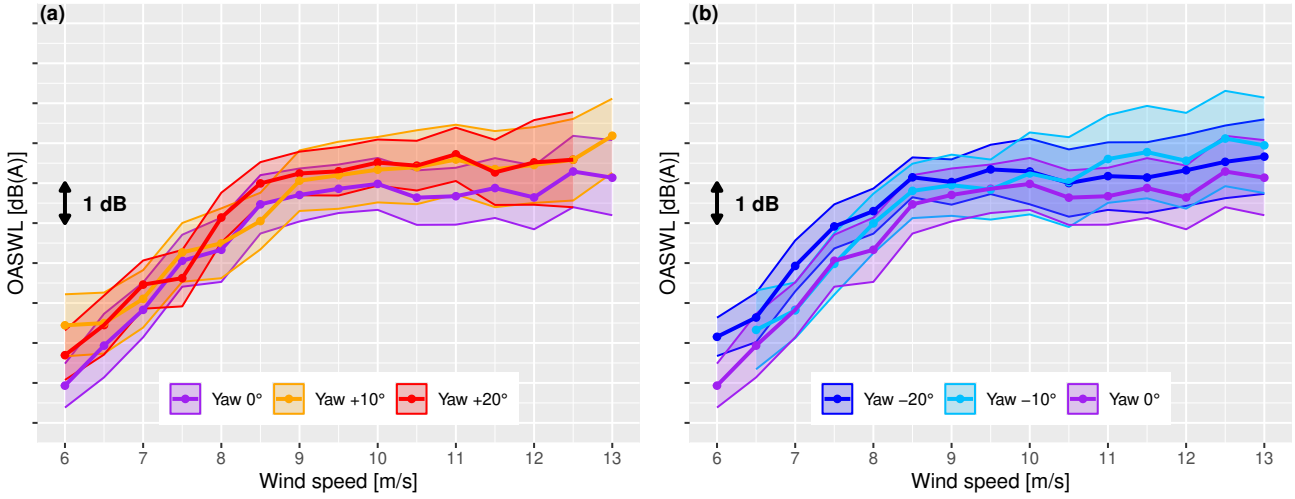

Figure 19. Turbine overall A-weighted sound power level (OASWL) as a function of wind speed for positive (a) and negative (b) yaws. The shaded ribbon represents one standard uncertainty associated to each OASWL value $u_{L_{WA,\{v,\beta\}}}$, while the point markers indicate the mean value $L_{WA,\{v,\beta\}}$. For wind speed bins and yaw ~~offset~~ misalignment cases with too few observer positions, the point is omitted.

process and alter its directivity trace on ground SLMs. Conversely, TBL-TE noise is produced by the interaction of a turbulent boundary layer ~~– trailing edgenoise, which is prominent at high frequencies. These distinct sources may be differently affected~~ (at the surface of the blade) and the trailing edge. The process is somewhat more local and may be less influenced by the yaw ~~misalignment~~configuration.

Estimates of turbine's OASWL derived using Eqs. 7 and 8 are presented in Fig. 19 for various yaw ~~offset~~ misalignment angles, both positive (left panel) and negative (right panel). All empirical sound power curves exhibit a consistent structure, characterized by a linear increase between 6 m/s and 9 m/s, followed by a plateau at higher wind speeds, as expected for this turbine. For most wind speed bins, the aligned configuration $\beta = 0°$ is the less noisy configuration. In contrast, configurations with ~~non-zero yaw offsets~~ yaw misalignment tend to exhibit more elevated sound power levels. To evaluate the statistical significance of these observations, four inverse-variance weighted paired t-tests were conducted using Eqs. 10 and 11. Each test compares the sound power curve for a misaligned configuration $L_{WA,\{v,\beta\neq 0°\}}$ against the reference aligned configuration $L_{WA,\{v,\beta=0°\}}$. The result, summarized in Tab. 5, indicate that for yaw angles of $\beta = -20°, +10°, 20°$, the differences are statistically significant ($p < 0.05$). These configurations exhibit a consistent increase in OASWL of approximately 0.5 to 0.7 dB(A). Accordingly, it can be concluded that these misaligned settings are slightly noisier than the baseline configuration, with an average increase in sound power of approximately 0.6 dB(A).

The slice summation described in Eq. 7 can be independently computed for each 1/3-octave band, yielding the turbine's sound power level ~~(SWL)~~ spectra.These spectra are presented in Fig. 20 for various yaw ~~offset~~ misalignment configurations. Consistent with the OASPL analysis, all ~~yawed~~ yaw misaligned configurations exhibit higher spectral levels compared to the

Table 5. T-test results for the offset in sound power level curves compared to the aligned case.

Yaw ~~offset~~ misalignment β (°)	$\overline{\Delta L}_{WA}$ (dB(A))	95% Confidence Interval (dB(A))	p-value
-20	+0.7	[0.25; 1.21]	0.003
-10	+0.5	[-0.08; 1.09]	0.09
10	+0.6	[0.07; 1.12]	0.03
20	+0.6	[0.14; 1.13]	0.01

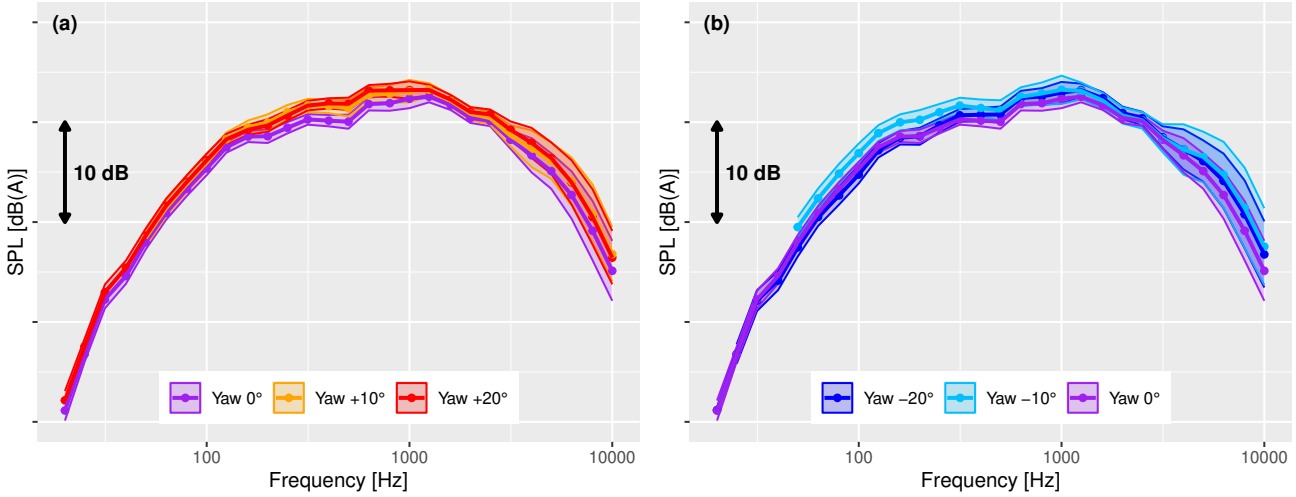

Figure 20. Turbine sound power level spectra at $v = 11$ m/s for positive (a) and negative (b) ~~yaws~~yaw angles. The shaded ribbon represents one standard uncertainty.

baseline (aligned) case. The increase is particularly notable in the low to mid-frequency range (200 – 1250 Hz) as well as in the high-frequency range ($f > 5$ kHz). As previously discussed in the analysis of Fig.18, this pattern suggests that the dominant noise generation mechanisms are differentially influenced by turbine yaw misalignment. At the wind farm level, the observed slight increase in TI noise levels under misaligned yaws may be compensated by the fact that wake-turbine interactions are basically avoided in WFFC control strategies, a situation which typically produces large TI noise increases.

The results presented here may be compared ~~to~~ with the extensive noise measurement campaign conducted at NREL by Hamilton et al. (2021) near a 77 m ~~, diameter~~diameter, 1.5 MW industrial wind turbine ~~submitted~~ subjected to a yaw ~~offsets~~ misalignment ranging from -18° to +25°. ~~Their study focused on the downstream region of the turbine with a viewing angle of approximately 100°. A comparison of noise levels at *fixed* ground positions with and without yaw generally revealed a slight decrease of 1 to 2 dB at moderate yaw angles. In contrast,~~ They reported a general *decrease* in SPL by 2 to 3 dB for intermediate yaw offsets (10° and 18°). At more extreme yaw misalignments of -18° and 25°, even larger noise decreases

were observed, reaching up to -5 dB compared to the non-steered configuration. At first glance, this appears to contradict the present study~~observed a slight increase~~ , which reports a slight *increase* of +0.6 dB in noise power levels under ~~yaw conditions. This discrepancy may be attributed to differences in turbine model, size and control system. Additionally, a partial view on the directivity pattern and its rotation may result in local sound pressure level decreases which may be attributed to an apparent sound power level decrease~~yawed conditions. However, several aspects should be considered before drawing such a conclusion.

First, the turbines under investigation are from different manufacturers and their designs differ significantly. The rated powers differ by 31%, the diameters by 30%, and the blade geometries are also dissimilar. For instance, suction side flow recirculation may occur for one blade design under yaw, but not on another, with potentially significant consequences for noise emissions. To date, there is no general evidence supporting the assumption that the effect of wake steering on noise emissions is model-independant. More specifically, the concerned turbine controllers[1] appear to response differently to the yaw misalignment. Hamilton et al. (2021) noticed a reduction in rotor speed under yawed operation at low and moderate wind speeds $v \leq 10$ m/s, which they identified as the main cause of the observed noise reduction. In contrast, in the present study, no systematic change in rotor speed was observed under yaw misalignment. Therefore, differences in turbine control strategies could plausibly explain why no noise level reduction is observed here. However, this explanation only applies to wind speeds below 10 m/s, whereas the NREL study reports noise reductions at higher wind speeds as well.

Second, the NREL study was limited to the downstream region with a viewing angle of approximately 100° and an angular resolution of 25°. Under such conditions, variations in measured noise levels cannot be directly attributed to changes in turbine emissions alone, as the rotation of the directivity pattern also plays a role. In particular, SLMs falling in the noise dip – depending on their position and the yaw angle – may record an apparent noise reduction, even if the total turbine noise power remains unchanged. Indeed, in the NREL study, SLMs consistently showing SPL reductions under yaw misalignment were located closer to the rotor plane than in the non-steered configuration. This ambiguity motivated the use of a larger number of SLMs in the present set-up, uniformly distributed on a circle centered on the wind turbine.

Finally, it should be noted that the largest noise reduction reported in NREL study occurs at 25° yaw, a configuration that is not investigated here. Although the amount of data, the wind speed range and pre- and post-processing strategies are broadly comparable between the two studies, it is suggested that the differing conclusions arise from differences in turbine control strategies, experimental setups and yaw misalignment ranges. Another point of comparison is provided by Bonsma et al. (2019) . Using two SLMs, they monitored noise levels within a wind farm equipped with six industrial turbines operated under WFFC. They reported no statistically significant difference in the sound levels between regular and yaw-misaligned operation. While this setup – featuring six steered turbines but only two sensors – is relevant from a wind farm operator's perspective, it is not suitable for detecting small variations in individual turbine noise power levels of the order of 0.5 dB. This limitation again arises because fixed sensors are influenced by both the rotation of the directivity pattern rotation and potentially small variations in noise power; the latter requiring a larger amount of data and sensors to be reliably detected. Finally, both studies from the

[1] Turbine controllers define the operating point (via torque and blade tip speed settings) as a function of the incoming wind speed. Their design details are typically not disclosed to wind farm operators

literature are generally consistent with the present work in indicating that the application of WFFC does not lead to a large increase in sound power emissions that could compromise the objective of enhancing power production.

5 Conclusions

A novel acoustic measurement campaign was conducted around an industrial 2.2 MW wind turbine, involving 24 ground-based sound level meters and multiple lidar devices to monitor incoming wind speed and direction. The experiment encompassed a wide range of wind conditions, enabling the construction of detailed directivity patterns across the turbine's full operational range. Modifications to the IEC standard methodology were proposed to leverage the advantages of this multi-point measurement setup. Furthermore, the turbine was operated both under standard alignment control and with intentional yaw ~~offsets (~~misalignment (angles ranging from $-20°$ to $+20°$), in order to investigate sound power variations associated with wake steering strategies.

Measurements conducted under non-steered conditions reveal that the turbine generally exhibits a two-lobe directivity pattern aligned with the nacelle axis. However, in most tested configurations, the axial downwind direction does not correspond to the direction of maximum emissivity, with differences ranging from 0.7 to 1.6 dB(A), contrary to predictions from most semi-empirical and analytical wind turbine noise models. Furthermore, the measured directivity patterns display asymmetry, with a statistically significant offset of +0.6 dB on the downstroke side compared to its symmetrical upstroke counterpart, and +0.4 dB on the downwind side relative to the upwind side. Spectral comparisons in the off-axis directions of maximum OASPL ($\theta = +45°$ and $\theta = +135°$) reveal a pronounced broadband contribution around 1000 Hz, reduced sound pressure levels at low frequencies, and elevated levels at high frequencies ($f > 5$ Hz).

Acoustic curtailment plan are currently still derived assuming turbines are omnidirectional noise sources. By accounting for a more detailed directivity pattern in the design of those plans, wind farm operators could be able to develop much refined strategies that could in turn lead to significant energy gains over the full lifetime of a project.

When ~~a yaw offset~~ yaw misalignment is applied, the directivity pattern rotates in alignment with the turbine's axis, exhibiting increased complexity with additional lobes and dips compared to standard operating conditions. An increase in the turbine's sound power level~~(SWL)~~, estimated from the multi-point ground-based acoustic footprint, is observed -— approximately +0.6 dB(A), independently of the actual yaw angle value. This increase is particularly pronounced in the low-frequency range (below 1000 Hz) and the high-frequency range (above 5000 Hz), suggesting that yaw misalignment differentially affects the primary noise generation mechanisms.

This first of ~~his~~ its kind experiment underlines the complexity of multi-objective WFFC and the need for more detailed analytical noise models. Indeed, while wake steering has shown consistent results for mitigating wake effects and improving overall wind farm production, the increased noise emissions could lead to more constraining acoustic curtailment plan that will have the opposite effect on farm performance. Reliable models must be developed so that operators can weight the costs and benefits of their choices, and make better informed decision. Future work in the scope of the TWAIN project will focus on the

validation of more advanced turbine noise emission models using the data generated through this experiment, which will later be used in a case study combining wake steering and noise optimization.

Data availability. Since the experiment was realized on a commercial wind turbine, the data used in this research cannot be made available.

Author contributions. The TWAIN acoustic campaign was designed and realized by TD and AF. Wind related data were post-processed by TD and acoustic related data by AF. The methodology detailed in Sect. 3 was derived conjointly by TD and AF. TD wrote sections 1, 2 and 3 and AF wrote sections 4 and 5. Both authors reviewed and edited the manuscript.

Competing interests. The authors declare that they have no conflict of interest.

Acknowledgements. The TWAIN acoustics campaign is realized under the TWAIN project, funded by the European Union's Horizon Europe research and innovation program with grant agreement no. 101122194.

We would like to thank Florent Bruneau and all the Echopsy team for their great support in setting up and conducting the field test. Additionally, we would like to acknowledge four other ENGIE Green colleagues: Warren Herbaut for solving all operational constraints related to the preparation of the campaign, Assia Achhibat for the help in the data preprocessing, Paul Mazoyer for the tip allowing us to properly combine data from multiple ~~microphones~~ SLMs at a given relative position and Colin Le Bourdat for the general support of this work.

References

Astolfi, D., Gao, L., Pandit, R., and Hong, J.: Experimental Analysis Of The Effect Of Static Yaw Error On Wind Turbine Nacelle Anemometer Measurements, in: 2023 IEEE International Conference on Environment and Electrical Engineering and 2023 IEEE Industrial and Commercial Power Systems Europe, pp. 1–6, https://doi.org/10.1109/EEEIC/ICPSEurope57605.2023.10194644, 2023.

Bertagnolio, F., Fischer, A., Appel, C., Herr, M., Seel, F., Lutz, T., Boorsma, K., Schepers, G., Botero, M., Casalino, D., van der Velden, W., Sucameli, C., and Bortolotti, P.: Wind turbine noise code benchmark: A comparison and verification exercise, 2023.

Boersma, S., Doekemeijer, B. M., Gebraad, P. M., Fleming, P. A., Annoni, J., Scholbrock, A. K., Frederik, J. A., and van Wingerden, J.-W.: A tutorial on control-oriented modeling and control of wind farms, in: 2017 American control conference (ACC), pp. 1–18, IEEE, 2017.

Bonsma, I., Gara, N., and Howe, B.: Intentional Yaw Misalignment and the Effects on Wind Turbine Noise, Canadian Acoustics, 47, 66–67, 2019.

Borraccino, A., Schlipf, D., Haizmann, F., and Wagner, R.: Wind field reconstruction from nacelle-mounted lidar short-range measurements, Wind Energy Science, 2, 269–283, https://doi.org/10.5194/wes-2-269-2017, 2017.

Bossanyi, E. and Ruisi, R.: Axial induction controller field test at Sedini wind farm, Wind Energy Science, 6, 389–408, https://doi.org/10.5194/wes-6-389-2021, 2021.

Buck, S., Oerlemans, S., and Palo, S.: Experimental characterization of turbulent inflow noise on a full-scale wind turbine, Journal of Sound and Vibration, 385, 219–238, 2016.

Damiani, R., Dana, S., Annoni, J., Fleming, P., Roadman, J., van Dam, J., and Dykes, K.: Assessment of wind turbine component loads under yaw-offset conditions, Wind Energy Sci., 3, 173–189, https://doi.org/10.5194/wes-3-173-2018, 2018.

Dana, S., Ivanov, H., and Doubrawa, P.: Lifetime fatigue response due to wake steering on a pair of utility-scale wind turbines, Journal of Physics: Conference Series, 2265, 022 106, https://doi.org/10.1088/1742-6596/2265/2/022106, 2022.

Doekemeijer, B. M., Kern, S., Maturu, S., Kanev, S., Salbert, B., Schreiber, J., Campagnolo, F., Bottasso, C. L., Schuler, S., Wilts, F., Neumann, T., Potenza, G., Calabretta, F., Fioretti, F., and van Wingerden, J.-W.: Field experiment for open-loop yaw-based wake steering at a commercial onshore wind farm in Italy, Wind Energy Science, 6, 159–176, https://doi.org/10.5194/wes-6-159-2021, 2021.

Finez, A., Duc, T., , and Le Bourdat, C.: Measurement of directivity patterns of a commercial wind turbine under yaw offset, in: 11th Edition of the International Conferences on Wind Turbine Noise: Conference Proceedings, pp. 270–285, Copenhagen, Denmark, https://doi.org/10.11581/08042886-dea0-4511-b4bd-6c5403125735, 2025.

Fleming, P., Annoni, J., Shah, J. J., Wang, L., Ananthan, S., Zhang, Z., Hutchings, K., Wang, P., Chen, W., and Chen, L.: Field test of wake steering at an offshore wind farm, Wind Energy Science, 2, 229–239, https://doi.org/10.5194/wes-2-229-2017, 2017.

Fleming, P., King, J., Dykes, K., Simley, E., Roadman, J., Scholbrock, A., Murphy, P., Lundquist, J. K., Moriarty, P., Fleming, K., van Dam, J., Bay, C., Mudafort, R., Lopez, H., Skopek, J., Scott, M., Ryan, B., Guernsey, C., and Brake, D.: Initial results from a field campaign of wake steering applied at a commercial wind farm – Part 1, Wind Energy Science, 4, 273–285, https://doi.org/10.5194/wes-4-273-2019, 2019.

Fleming, P., King, J., Simley, E., Roadman, J., Scholbrock, A., Murphy, P., Lundquist, J. K., Moriarty, P., Fleming, K., van Dam, J., Bay, C., Mudafort, R., Jager, D., Skopek, J., Scott, M., Ryan, B., Guernsey, C., and Brake, D.: Continued results from a field campaign of wake steering applied at a commercial wind farm – Part 2, Wind Energy Science, 5, 945–958, https://doi.org/10.5194/wes-5-945-2020, 2020.

Fleming, P., Sinner, M., Young, T., Lannic, M., King, J., Simley, E., and Doekemeijer, B.: Experimental results of wake steering using fixed angles, Wind Energy Science, 6, 1521–1531, https://doi.org/10.5194/wes-6-1521-2021, 2021.

Göçmen, T.: Possible Power Estimation of Down-Regulated Offshore Wind Power Plants, Ph.D. thesis, Technical University of Denmark, 2016.

Guillemin, F., Nguyen, H.-N., Sabiron, G., Di Domenico, D., and Boquet, M.: Real-time three dimensional wind field reconstruction from nacelle LiDAR measurements, in: Journal of Physics: Conference Series, vol. 1037, p. 032037, IOP Publishing, 2018.

Hamilton, N., Bortolotti, P. E., Jager, D., Guo, Y., Roadman, J. M., and Simley, E.: Aeroacoustic Assessment of Wind Plant Controls, Tech. rep., National Renewable Energy Lab.(NREL), Golden, CO (United States), 2021.

Harrison, M., Vishwakarma, P., Williams, R., Smith, G., Downes, P., King, J., and Landberg, L.: Results of the first DNV joint industry project on wind farm flow control, in: Wind Energy Science Conference 2025, Nantes, France, 2025.

Howland, M. F., Quesada, J. B., Martínez, J. J. P., Larrañaga, F. P., Yadav, N., Chawla, J. S., Sivaram, V., and Dabiri, J. O.: Collective wind farm operation based on a predictive model increases utility-scale energy production, Nature Energy, 7, 818–827, 2022.

IEC: IEC 61400–11-1, Wind turbines - part 11-1: Acoustic noise measurement techniques, Tech. rep., International Electrotechnical Commission, 2012.

IEC: IEC 61400–12-1, wind turbines - part 12–1: Power performance of electricity producing wind turbines, Tech. rep., International Electrotechnical Commission, 2017.

Kanev, S.: AWC validation methodology, Tech. Rep. R11300, TNO, 2020.

Mazoyer, P. and Boquet, M.: Retrieving wind speed at constant height above ground level in complex terrain with a Wind Iris 4-beam nacelle Lidar, in: Wind Europe Summit 2016, Hamburg, Germany, https://windeurope.org/summit2016/conference/allposters/PO263.pdf, 2016.

McKay, P. M., Carriveau, R., Ting, D. S.-K., and Johrendt, J. L.: Global sensitivity analysis of wind turbine power output, Wind Energy, 17, 983–995, 2014.

Meyers, J., Bottasso, C., Dykes, K., Fleming, P., Gebraad, P., Giebel, G., Göçmen, T., and van Wingerden, J.-W.: Wind farm flow control: prospects and challenges, Wind Energy Science, 7, 2271–2306, https://doi.org/10.5194/wes-7-2271-2022, 2022.

Nyborg, C. M., Fischer, A., Réthoré, P.-E., and Feng, J.: Optimization of wind farm operation with a noise constraint, Wind Energy Science, 8, 255–276, https://doi.org/10.5194/wes-8-255-2023, 2023.

Oerlemans, S. and Schepers, J. G.: Prediction of wind turbine noise and validation against experiment, International journal of aeroacoustics, 8, 555–584, 2009.

Oerlemans, S., Sijtsma, P., and Méndez López, B.: Location and quantification of noise sources on a wind turbine, Journal of Sound and Vibration, 299, 869–883, https://doi.org/https://doi.org/10.1016/j.jsv.2006.07.032, 2007.

Okada, Y., Yoshihisa, K., Higashi, K., and Nishimura, N.: Horizontal directivity of sound emitted from wind turbines, Acoustical Science and Technology, 37, 239–246, 2016.

Raach, S., Schlipf, D., Haizmann, F., and Cheng, P. W.: Three dimensional dynamic model based wind field reconstruction from lidar data, in: Journal of Physics: Conference Series, vol. 524, p. 012005, IOP Publishing, 2014.

Roger, M. and Moreau, S.: Extensions and limitations of analytical airfoil broadband noise models, International Journal of Aeroacoustics, 9, https://doi.org/10.1260/1475-472X.9.3.273, 2010.

Romani, G., Casalino, D., and Velden, W. v. d.: Numerical Analysis of Airfoil Trailing-Edge Noise for Straight and Serrated Edges at Incidence, AIAA Journal, 59, 2558–2577, https://doi.org/10.2514/1.J059457, 2021.

Rott, A., Höning, L., Hulsman, P., Lukassen, L. J., Moldenhauer, C., and Kühn, M.: Wind vane correction during yaw misalignment for horizontal-axis wind turbines, Wind Energy Science, 8, 1755–1770, https://doi.org/10.5194/wes-8-1755-2023, 2023.

Shahar, D. J.: Minimizing the variance of a weighted average, Open Journal of Statistics, 7, 216–224, 2017.

Simley, E., Fleming, P., Girard, N., Alloin, L., Godefroy, E., and Duc, T.: Results from a wake-steering experiment at a commercial wind plant: investigating the wind speed dependence of wake-steering performance, Wind Energy Science, 6, 1427–1453, https://doi.org/10.5194/wes-6-1427-2021, 2021.

Tian, Y. and Cotté, B.: Wind Turbine Noise Modeling Based on Amiet's Theory: Effects of Wind Shear and Atmospheric Turbulence, Acta Acustica united with Acustica, 102, 626–639, https://doi.org/10.3813/AAA.918979, 2016.

Tukey: Exploratory data analysis, vol. 2, Springer, 1977.

TWAIN: Integrated, Value-based, and Multi-objective Wind Farm Control powered by Artificial Intelligence, https://twainproject.eu/, accessed on 2026-05-29, 2023.

van der Hoek, D., Kanev, S., Allin, J., Bieniek, D., and Mittelmeier, N.: Effects of axial induction control on wind farm energy production - A field test, Renewable Energy, 140, 994–1003, https://doi.org/10.1016/j.renene.2019.03.117, 2019.

van Wingerden, J. W., Fleming, P. A., Göçmen, T., Eguinoa, I., Doekemeijer, B., Dykes, K., Lawson, M., Simley, E., King, J., Astrain, D., et al.: Expert elicitation on wind farm control, in: Journal of Physics: Conference Series, vol. 1618, p. 022025, IOP Publishing, https://doi.org/https://doi.org/10.5194/wes-6-159-2021, 2020.

Willis, H.: Curtailment strategies due to environmental constraints in France. Evolution of their occurrence and impact over time, in: WindEurope Annual Event 2023, Copenhagen, Denmark, https://www.eoltech.fr/media/pdfs/PO038.pdf, 2023.